Chapter 1

IceCube: Submm-Wave Technology Development for Future Science on a CubeSat

Dong L. Wu, Jeffrey R. Piepmeier, Jaime Esper, Negar Ehsan, Paul E. Racette, Thomas E. Johnson, and Brian S. Abresch
NASA Goddard Space Flight Center (GSFC)
Greenbelt, Maryland, USA

Eric Bryerton
Virginia Diodes, Inc. (VDI)
Charlottesville, Virginia, USA

1.1 Introduction

Clouds play important roles in Earth's climate and weather systems through interactions with atmospheric processes in radiation, dynamics, latent heat release, and precipitation at a wide range of spatiotemporal scales. Clouds are the leading source of uncertainties in climate/weather prediction [e.g., Randall et al., 2007, IPCC, 2013]. Ice clouds, in particular, have been used as a tuning parameter in global circulation models (GCMs) to achieve model agreement with observations at the top of the atmosphere (TOA) for radiation budget and at the bottom for precipitation. Clouds in the GCMs have been less realistically represented, largely because of inaccurate ice cloud measurements and poorly-constrained cloud processes in the model. As a result, there is a wide spread in the cloud ice amount simulated from GCMs [e.g., Waliser et al., 2009; Jiang et al., 2012; Li et al., 2016].

Submillimeter (submm) wave remote sensing at 200-1000 GHz is capable of penetrating clouds to measure cloud ice mass and microphysical properties in the middle-to-upper troposphere, filling the sensitivity gap not covered by visible (VIS)/infrared (IR) and low-frequency microwave (MW) sensors (10-183 GHz). However, risks and potentially high costs remain as an obstacle for enabling future science missions for high frequency receivers. For decades NASA has made a significant effort to advance submm-wave technologies and the development of spaceflight systems for science applications. The IceCube project is the latest of NASA's effort to advance the technology readiness level (TRL) of a commercial 883-GHz cloud radiometer.

Access to space is challenging and costly. In the past NASA has been relying primarily on sounding rockets, high-altitude balloons, and the International Space

Station (ISS) as a vehicle to validate new technologies prior to their use in a science mission. This validation step is necessary because of the stringent spaceflight conditions imposed on instrument components and systems, some of which cannot be fully tested on the ground or in airborne systems. Sounding-rocket or balloon flight tests sometimes may not even be sufficient as they are often short and do not address endurance and other extreme aspects of the spaceflight environment. While spaceflight validation is critical for risk and cost reduction, it has also been recognized that a new approach is needed, one that shortens the development cycle of space technologies.

Emerging CubeSat opportunities are transforming the means by how new space technologies are demonstrated and validated; through small standardized satellites, fast-track development, and low-cost access to space. Once in orbit, CubeSats are able to carry the in-situ sensors or remote-sensing instruments into the real spaceflight environment that will be similar to the future science missions but testing for lifetime, stability, and endurance. The NASA In-Space Validation of Earth Science Technologies (InVEST) program has been established to validate and reduce the risk of new technologies for future Earth science missions. In addition, NASA established an agency-wide Small Spacecraft Technology Program (SSTP) to enhance/expand the capabilities of small spacecraft through spaceflight demonstration and testing. IceCube is one of the earliest experiments intended to evaluate and use the CubeSat platform to advance space technology. The IceCube 883-GHz instrument and 3U CubeSat systems were developed at Goddard Space Flight Center (GSFC) over a period of ~3 years, using commercial subsystems and COTS components.

This paper provides an overview of the IceCube project, including its payload and CubeSat development and performance in spaceflight. Like other CubeSat missions, IceCube has a goal to miniaturize remote-sensing sensors and to increase the reliability of small satellites. Using small, modular and standardized spacecraft along with mineaturized sensor units, we hope to advance Earth and planetary sciences by forming a space sensor constellation or sending scout-units from a mothership for targeted science investigations. IceCube is a pathfinder at NASA that infuses and integrates small spacecraft technologies to merge it with its larger mission goals. Effective government-commercial partnerships have played a key role in meeting the fast-track, low-cost requirements. Early lessons learned from IceCube will benefit the CubeSat community as well as the science investigations that plan to use nano/microsatellites.

1.2 IceCube System Overview

1.2.1 Objective and Goal

The primary objective of IceCube is to raise the TRL of a commercial 883-GHz cloud radiometer from 5 to 7 by flying and validating the technology in a relevant spaceflight environment. Successful demonstration of the commercial 883-GHz cloud radiometer reduces the risks and costs of future Earth Science missions on cloud ice observations. In addition, the technology enables a host of applications in planetary and heliophysics sciences that use submm-wave remote sensing. IceCube leverages the recent availability and advances of commercial submm-wave technology to achieve low-cost spaceflight demonstration of a cloud radiometer at 883 GHz. Emerging CubeSat platforms provide fast-track access to space, which greatly shortens the development cycle of spaceflight technology demonstration. The IceCube team employs the sub-Class-D system-engineering approach to test and verify the key subsystems and components, including commercial on off-the-shelf (COTS) parts, to assure mission success.

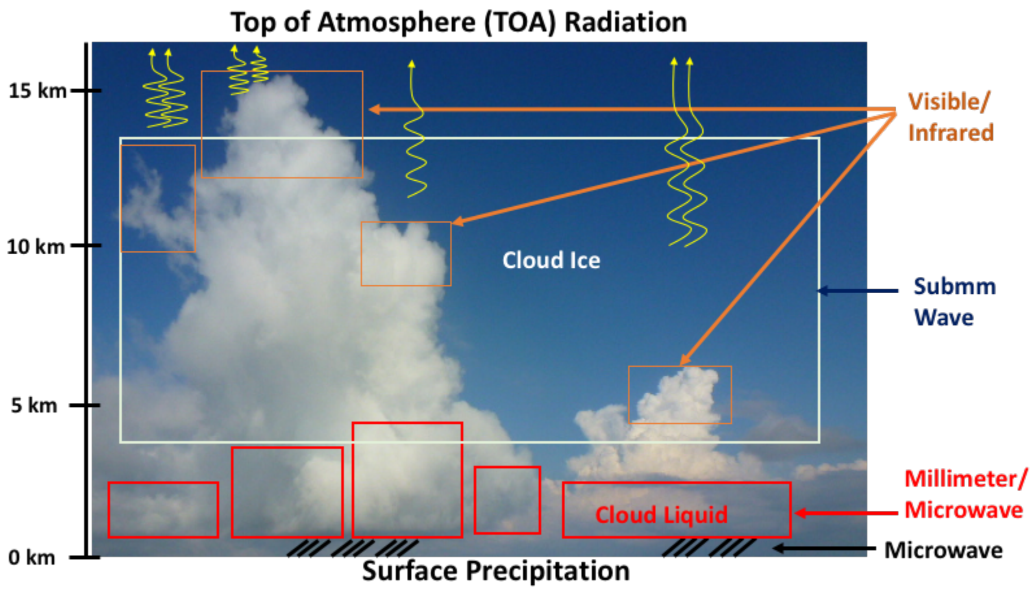

Fig. 1-1. Submm-wave sensors provide the needed sensitivity to fill the gap in current satellite observations to better understand cloud processes and their interactions with radiation and precipitation. Accurate measurements of cloud ice distributions and variations in the middle and upper troposphere will help to reduce deficiency and uncertainty about clouds in the models.

Submm wave remote sensing has the advantage of filling the sensitivity gap between MW and VIS/IR remote sensing. The technique provides adequate ice cloud penetration as well as sensitivity to cloud ice mass and microphysical properties in the middle-to-upper troposphere. As shown in Fig. 1-1, a dedicated suite of mm- and submm-wave cloud radiometers can provide a critical cloud ice measurement to fill the sensitivity gap not covered by VIS/IR and MW sensors [Evans, et al., 2002; Buehler et al., 2012]. Of particular interest to ice cloud remote sensing is the 860-900 GHz spectral window, which provides not only good sensitivity to cloud scattering but also allow sufficient penetration to measure mid-tropospheric cloud ice. Cloud observations at 1-5 THz becomes difficult because of the increasing atmospheric attenuation from continuum absorption.

Ice water path (IWP) is a key parameter to characterize cloud radiative and hydrological properties. Despite great advances from CloudSat radar and other satellite sensors [Stephens et al., 2008], global IWP measurements still differ from each other by a factor of 2 or greater, largely because of uncertainties about the microphysical property assumptions used in cloud ice retrieval algorithms [Wu et al., 2009; Eliasson et al., 2011].

To improve cloud ice measurements, GSFC has been working with Virginia Diodes, Inc. (VDI) to develop receivers that span from 100 GHz to 1 THz, which has become the foundation of GSFC's airborne Compact Scanning Submillimeter-wave Imaging Radiometer (CoSSIR) [Zhang and Monosmith, 2008]. Designed as both a conical and cross-track imager with six receivers centered at 183, 220, 380, 640 V&H, and 874 GHz and eleven channels, CoSSIR was flown on NASA's ER-2 aircraft. The data from the CoSSIR channels showed that the accuracy of cloud IWP retrievals could be improved over a wide dynamic range between ~10 g/m^2 and 10,000 g/m^2 [Evans, et al., 2012]. Of all CoSSIR radiometer frequencies, the 874-GHz channel is the most sensitive to IWP, yet poses the greatest technical risk and highest development cost for spaceflight.

With the expectation that the CoSSIR submm-wave radiometers would perform in space, IceCube was funded by NASA to make a fast-track spaceflight demonstration and validation of the VDI 883-GHz receiver for cloud ice observations. The top objective of IceCube is to retire the risks associated with the VDI receiver by raising its TRL from 5 to 7. VDI has commercialized the 874-GHz receiver as well as other radiometers at submm-wave frequencies from their VNA Extender line. Yet, the stability of these VDI receivers in space is uncertain. To characterize and monitor receiver performance, the IceCube radiometer design allows experiments in spaceflight to switch on and off the frontend mixer at a rate of 10 kHz and to inject a noise source in the backend intermediate frequency (IF) chain for IF gain monitoring. Since the VDI 883-GHz receiver is compact, the project chose to use a 3U CubeSat for a short (28-days) technology demonstration.

To simplify system design and reduce mission risk, IceCube eliminates the conventional scan mirror mechanism used in microwave radiometers for radiometric calibration and atmospheric observations. Instead, it spins the spacecraft to obtain periodic views between cold space and Earth's atmosphere. IceCube is essentially a free-running radiometer. The frequent space views provide the needed background calibration to track the receiver thermal and temporal variations. Using modeled clear-sky Earth radiances, radiometric calibration can be done to derive the instrument gain/sensitivity and detect cloud scattering.

1.2.2 Measurement Technique

MW radiation as seen from space is primarily from the Earth's surface and atmospheric gases. There are spectral windows where no major absorption lines from atmospheric gases are present in the spectrum. Both the Earth's surface and atmospheric gases radiate like a grey body (blackbody with imperfect emissivity

ε), which produces a MW radiance characterized by a brightness temperature (T_b). T_b can be related to the physical temperature (T) of the emission source ($T_b = \varepsilon T$) and is typically warmer if it is near the surface and colder if it is from the upper troposphere. In the presence of ice clouds, MW radiation will be scattered by the clouds in all directions. The scattered T_b is generally lower than then the clear-sky T_b at nadir viewing from space, because it is a combination of upwelling warm T_b and downwelling cold space background (i.e., Cosmic Microwave Background, or CMB). The T_b of CMB is 2.73K at 0.1 GHz but becomes nearly zero at 883 GHz from Planck's black-body equation.

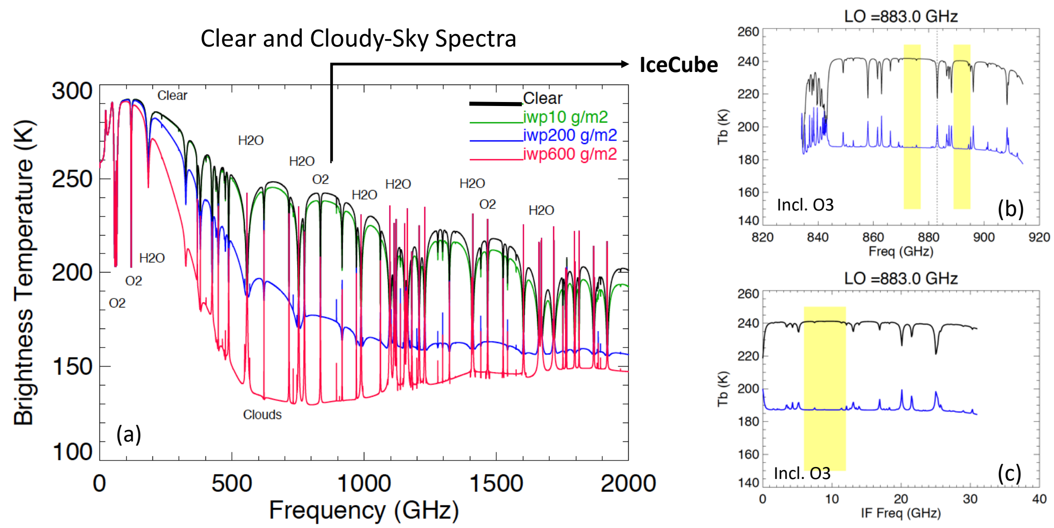

Fig. 1-2. (a) Cloud ice scattering at mm- and submm-wave frequencies from different IWPs. The 800-900 GHz region, one of the spectral windows where there are a fewer absorption line features from major atmospheric gases (i.e., O_2 and H_2O), allows radiation to penetrate deeper into the atmosphere for cloud ice measurements. The higher frequency channel is more sensitive to cloud scattering than those at lower frequencies. Beyond 1 THz, the increasing H_2O continuum absorption begins to attenuate the cloud scattering. (b) Detailed spectrum at 830-910 GHz that includes O_3 absorption lines. IceCube is designed to minimize impacts of atmospheric O_3 variability by setting the local oscillator frequency at 883 GHz. The yellow strips denote the receiver's upper and lower sidebands. (c) The IF spectrum in the IceCube's doube-sideband receiver. The yellow strip denotes the IF band of IceCube.

The effects of cloud scattering on MW radiance is shown in Fig. 1-2. The cloud-inducedreduction in T_b depends on the amount of cloud ice, or IWP, in the upper troposphere. A T_b reduction is more readily seen at the spectral windows than near the atmospheric line features, because atmospheric gaseous absorption tends to attenuate the cloud scattering effects that come from the troposphere. In the case of a very strong atmospheric absorption, such as those from O_2 where the absorption occurs in the stratosphere, the MW radiation has little sensitivity to clouds or any emissions in the troposphere. The spectral window near 883 GHz is perhaps the highest band in MW to effectively measure cloud-included T_b

reduction, beyond which the cloud scattering effect starts to decrease due to the increasing continuum absorption.

Ozone emission lines are not plotted in the full spectrum [Fig.1-2a], because they are everywhere in this spectral region. However, atmospheric ozone does produce absorption that would attenuate cloud scattering signals observed from space, therefore its effects need to be taken into account for designing a cloud observing system. As shown in the detailed spectrum near 883 GHz in Fig. 1-2 (b and c), the design of IceCube cloud radiometer chose the local oscillator (LO) frequency at 883 GHz, such that its upper (892 GHz) and lower (874 GHz) sidebands are both located within a window of ozone absorption lines.

1.2.3 The 883-GHz Cloud Radiometer

The 883 GHz receiver technology flown on IceCube was initially developed by VDI under a Small Business Innovation Research (SBIR) Phase II contract (NAS5-02107). Since the completion of Phase II in 2004, VDI has been successfully commercializing this technology. VDI has built over 100 receivers and sold over a dozen Vector Network Analyzer (VNA) Extenders in the 600 to 900 GHz frequency bands. GSFC worked previously with VDI in adapting its COTS 183 GHz receiver technology for the Global Precipitation Mission's Microwave Imager (GMI).

The IceCube 883 GHz radiometer technology is assessed at the system, subsystem, and component levels. The VDI-based 874 GHz radiometer system on CoSSIR is the first and only system known to us to have operated and observed the atmosphere to measure cloud ice from an aircraft (Evans, 2012). The subsystem comprises a LO amplifier/multiplier chain (AMC) and mixer, which both VDI and JPL have demonstrated at TRL 5 [Hesler, 2004; Thomas, 2008; Thomas, 2010]. AMC components in the 100-400 GHz range (IceCube requires a 441.5 GHz output) are developed by several organizations and are critical for radio astronomy in addition to remote sensing. Typically, planar Schottky varactor diodes have been used for multipliers, as is the case for the candidate VDI technology and for multipliers developed by JPL (e.g., [Schlecht, 2004]). For the mW-level output power capability required here, the TRL is 5; however, lower power output circuits have flown in space for pumping superconductor-insulator-superconductor (SIS) mixers on ESA's Herschel Space Observatory. This latter technology is not appropriate for NASA Earth remote sensing missions because of its cryogenic requirements. Among room temperature Schottky diode mixer components, there were only three designs at 874 GHz prior to IceCube: VDI's sub-harmonic mixer (Hesler, 2004); JPL's sub-harmonic mixer (Thomas, 2008); and JPL's fundamental balanced mixer (Thomas, 2010). Each of these achieved TRL 5 (relative to spaceflight), although via different means. The latter two have been laboratory tested at room and cryogenic temperatures. Of the three, VDI's is the only one commercially available.

Because of the potentially high technical risk and development cost of submm-wave receivers, adapting VDI's COTS receiver technology for spaceflight offers a clear path for reducing risk and cost. The CoSSIR experience using COTS components suggested that only minimal changes were required for the meeting spaceflight-quality standards.

The key technology in the 883 GHz receiver (mixer, doubler, and tripler) had achieved TRL 5 through the high-altitude partial vacuum environment of the ER-2 flights which were over a wide temperature range. This was not sufficient to achieve TRL 6 for spaceflight qualification testing (operational environment). The least mature technology from a flight perspective is the tripler and V-band power amplifier at TRL 5, which is fabricated at BAE Systems with a flight-qualified InP process for the National Radio Astronomy Observatory (NRAO). IceCube uses these components to save significant DC power (3W) in the LO chain compared to the original CoSSIR design. The same parts are used operationally in the ALMA (Atacama Large Millimeter/tarubmillimeter Array) telescope at 16,500 ft in the Atacama Desert plateau in northeastern Chile. The other IceCube cloud radiometer components are at TRL 6 or higher. The custom designed interface card utilizes screened parts that were procured through GSFC's electronic parts organization and leveraged existing flight project inventories. Technical risks of an electronics failure were further reduced with careful parts screening and thorough system level testing.

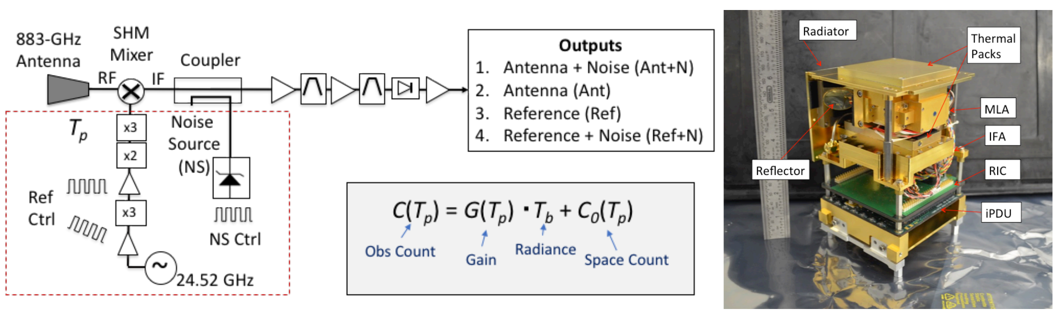

Fig. 1-3. Block diagram of the IceCube 883 GHz receiver. The IF calibration includes noise source injection ("Ant+N" and "Ref+N" states), LO modulation (switching between "Ant" and "Ref" states), and LO power monitoring isolates the response of submm receiver components. The thermal environment of the receiver system is monitored by a thermistor near the mixer (T_p). Measurements of four receiver states (Ant+N, Ant, Ref and Ref+N), sequencing through a 40ms time interval, are all output to diagnose the internal receiver noise as well as the radiance measurements from antenna. The image shows the IceCube instrument flight model (FM) integrated in a 1.5U volume, containing reflectors, MLA (Mixer LO Assembly), IFA (Intermediate Frequency Assembly), iPDU (instrument Power Distribution Unit), RIC (Receiver Interface Card), radiator and thermal paraffin packs.

A block diagram of the IceCube cloud radiometer system is shown in Fig. 1-3 with key instrument performance parameters listed in Table 1-1. The RF receiver is comprised of an offset parabola reflector with feedhorn, mixer, stable oscillator, RF multiplier chain, IF chain, video amplifier and detector. There are also supporting circuit boards including the instrument power distribution unit (iPDU), receiver interface card (RIC), and command and data handling (C&DH), which is shared with the CubeSat. There is no moving part in this radiometer. The radiometric calibration is achieved by spinning CubeSat at a rate of ~1° per second to yield periodic views between cold space and Earth. The modeled clear-sky radiances from Earth's atmosphere are used to provide the absolute radiometric calibration.

A block diagram of the IceCube cloud radiometer system is shown in Fig. 1-3 with key instrument performance parameters listed in Table 1-1. The RF receiver is comprised of an offset parabola reflector with feedhorn, mixer, stable oscillator, RF multiplier chain, IF chain, video amplifier and detector. There are also supporting circuit boards including the iPDU and C&DH, which is shared with the CubeSat. There is no moving part in this radiometer. The radiometric calibration is achieved by spinning CubeSat at a rate of ~1° per second to yield periodic views between cold space and Earth. The modeled clear-sky radiances from Earth's atmosphere are used to provide the absolute radiometric calibration.

In addition, the IceCube receiver experiment contains an internal IF calibration by operating the receiver frontend in a non-conversional way, imposing a 50% duty cycle on both the LO and noise source modulation ("Switching Sequence" in Fig. 1-3). IF calibration is achieved by noise injection and LO power modulation (and monitoring), providing the means of discriminating the calibration state of frontend components referenced to space-view observations. The instrument temperature fluctuations can affect the gain and noise figure of the IF-chain, excess noise ratio of the IF noise diode, LO-drive power, and the subharmonic mixer (SHM) conversion loss, thus, posing significant challenge to tracking the system response. By incorporating frequent two-point IF calibration, LO power monitoring and periodic observations of deep space with switched noise source injection, this instrument design allows us to track and validate the instrument response. In nominal operation, the instrument cycles through four measurement states in each 40-ms period: antenna (*Ant*), antenna + noise (*Ant*+*N*), IF reference (*Ref*), and IF reference + noise (*Ref*+*N*). Rather than using an IF switch, the LO power is modulated to effectively isolate the IF section. A noise source is coupled into the IF path during IF calibration and antenna measurements, thus, providing an RF-to-IF reference transfer. Four temperature sensors are used to monitor the thermal environment of sensitive components.

The radiometer frontend is comprised of a VDI's 883 GHz SHM pumped by a 441.5 GHz LO, which produces the lower and upper sidebands at 874 and 891 GHz respectively. The LO is sourced by 24.53-GHz (K-band) stable dielectric resonator oscillator (DRO), which is amplified and multiplied by a multichip module (MCM) containing a K-Band power amplifier MMIC, and frequency tripler and V-band power amplifier (PA) MMICs designed by NRAO/BAE for Atacama Large Millimeter wave Array (ALMA) telescope. This configuration saves 3W of DC power compared to the original CoSSIR design. The power output from this LO MCM drives the VDI frequency doubler and tripler, providing the ~2 mW required to pump the SHM. LO power is monitored at the second PA output using an inline microstrip directional coupler and V-band power detector.

The output of the mixer drives the IF chain (6-12 GHz), comprising an internal broadband noise source coupled into the IF path for calibration, followed by an isolator, LNA, band-pass filter, another gain stage, detector and video amplifier. The IF noise source uses components from the GMI X-band noise source design and the coupler and bandpass filter is designed and fabricated on the same standard microwave/RF substrate material using microstrip circuit topology. The video amplifiers are adopted from the Aquarius radiometer.

The antenna is an offset-fed paraboloid with a 15-mm aperture to produce a 1.8° half-power beamwidth, or 12.6 km footprint at nadir for the ISS orbit altitude (~400 km). Antenna beam spillover inside the instrument housing is minimized with absorber material placed on all critical flat surfaces. Its aperture is covered by a radome that is highly transparent in submm-wave but very reflective in infrared, to minimize impacts of external heat sources on the receiver.

Table 1-1. IceCube Radiometer Parameters

Reflector Antenna	Beam width: 1.8°; Beam efficiency: 93%
MLA LO (f_{LO})	883 GHz
MLA noise temp	3842 K @20°C
IFA BW	6.5 GHz
RIC	10 kHz 14-bit ADC
Normal operation	50% LO cycle
NEDT (1-secord)	0.3 K
Mass	1.3 kg
Daily Data Volume	< 3 MB
Total DC Power	5.6 W (50% LO cycle); 7.4 W (100% LO cycle)
Subsystem DC Power	3.55 W (MLA); 1 W (IFA); 2.5 W (iPDU); 0.3 W (RIC)

Note: LO (local oscillator), MLA (Mixer LO Assembly), IFA (Intermediate Frequency Assembly), iPDU (instrument Power Distribution Unit), RIC (Receiver Interface Card), noise equivalent differential temperature (NEDT), bandwidth (BW).

The 883-GHz mixer was delivered with a noise temperature of <5000 K at 20°C over the entire 6-GHz IF bandwidth. Including some conversion losses in the IF chain, the radiometer's NEDT is measured at ~0.3 K for a 1-second integration time in the laboratory. This receiver sensitivity is measured at ambient temperatures up to ~35°C before it degrades significantly. It is important to verify the IceCube cloud radiometer performance over a wide range of temperatures. Although the instrument should ideally operate at 20 ±2°C, using paraffin packs in the CubeSat to stabilize the thermal environment, heat generated from the instrument and spacecraft, as seen later in section 1.3.2, often saturates the capacity of paraffin packs. As a result, cycling the instrument on and off is needed to prevent the instrument from reaching a very hot temperature. Nevertheless, a large (10°C to +37°C) range of instrument temperature variations is typically experienced in the daily IceCube operation.

1.2.4 CubeSat Accommodation

Because of the compact design and modest power draw of the 883-GHz cloud radiometer, the entire system can be hosted on a 3-U CubeSat. IceCube's spacecraft is built internally at GSFC using COTS components (Table 1-2). As shown in Fig. 1-4, the bus consists of a 1.5U frame with the Attitude Determination and Control Subsystem (ADACS) attached to one end to complete a 2U unit. The ADACS is the XACT attitude control system from Blue Canyon Technologies (BCT). The BCT XACT has two modes: Sun Point (SP) and Fine Reference Point (FRP). SP is a safe mode to maintain spacecraft safety, while FRP is a high-performance mode for actual mission operations. The SP mode uses a minimal sensor suite to point a desired body-frame vector at the Sun, whereas the FRP mode uses the full sensor suite (e.g., GPS and star tracker) to accomplish a wide array of pointing objectives. The SP mode uses a coarse Sun sensor (CSS) as an absolute attitude reference to hold the spacecraft within 5° with respect to the Sun. The XACT 3-axis magnetometer is critical to momentum control in SP mode. In contrast, in FRP mode the momentum field is deduced from onboard time and ephemeris using a high-precision model of geomagnetic field.

Table 1-2. IceCube CubeSat (3U) Parameters

Flight Configuration	Spinning Axis: Sun Vector (day); Magnetic Field (night)
ADACS	BCT XACT
L3 Cadet	1 W (Tx Power), 450/468 MHz (Rx/Tx Frequency)
Ground Station	WFF UHF
Mass (w/ payload)	4.4 kg
Data Storage	4 GB
Clyde Space EPS	40 Whr (Battery)
Operation Power	8.4 W (Average), 18 W (Est. Max)
Subsystem DC Power	4.4 W (XACT), 0.5 W (EPS), 0.8 W (GPSAnt), 0.9 W (GPSRec), 1.7 W (SIC), 0.1 W (Pumpkin)
Design Lifetime	28 days

The overall IceCube system with payload fits within the 3U specification, with a total length of 340.5 mm, including 6.5mm posts on both ends, and a 100-mm by 100-mm body frame. Having the 3U split into bus and payload units takes full advantage of the CubeSat modular design, and the relatively minor volume inefficiency is offset by the ample volume margin available for subsystem boards. Bus components are also identified in Fig. 1-5. The current configuration leaves a 56mm axial margin (25+31mm) from the possible 340.5mm 3U CubeSat specification (20% margin). The stowed double-sided solar panels protrude 8mm from the 100mm CubeSat limit on either side and comply with the NanoRacks launcher dimension requirement.

IceCube has a 4.4kg mass and takes in ~18W power from its solar panels. Nonetheless, power management is an operational challenge because of the large DC power draw from the 883-GHz cloud radiometer. Reducing its duty cycle on the LO modulation helps to lower the payload power. In addition, the CubeSat is required to keep its solar panels towards the Sun and operate the instrument during daytime only, to give a sufficient margin to battery lifetime for a 28-day technology demonstration. An orbital power management scheme from beginning of life (BOL) to end of life (EOL) for each orbit is described in section 1.3.2.

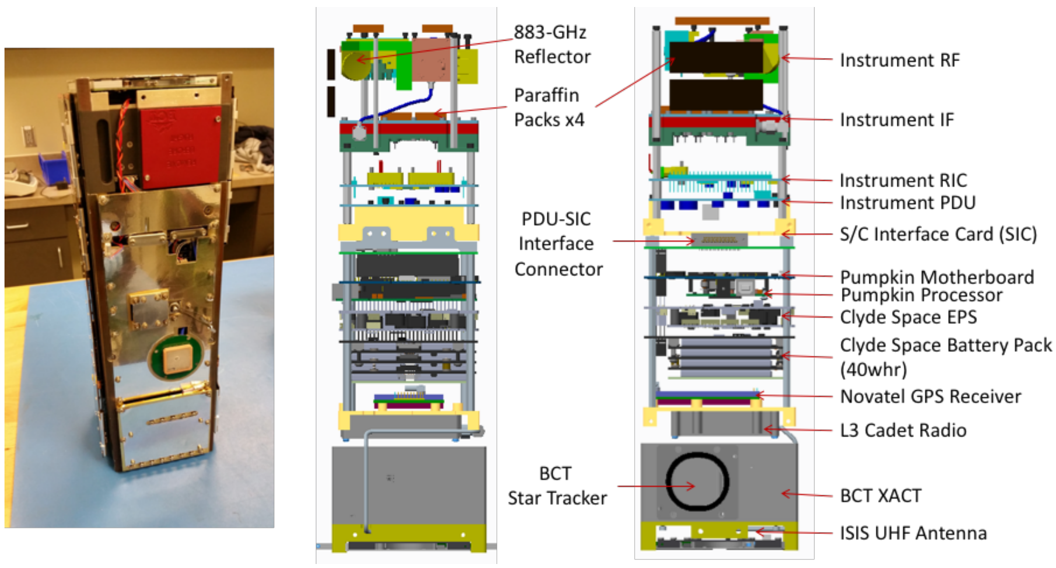

Fig. 1-4. Integrated IceCube 3U CubeSat (left), and interior layouts of spacecraft (S/C) structure and key subsystems (right).

Rigorous tests were carried out to encompass standard CubeSat requirements as well as the requirements for rideshare to ISS. Specific tests included vibration testing of the CubeSat to encompass the launch environment and thermal vacuum cycling over expected operating temperature range. The system did not perform any self-compatibility EMI/EMC testing due to schedule and budgetary constraints, but did pass an end-to-end communication test with the ground station.

During a 5-day system-level thermal vacuum (TVAC) test, IceCube successfully deployed its solar panels and powered on the instrument for its performance verification. The cloud radiometer was calibrated using three blackbody references at +40°C, -40°C and -179°C (LN2). But the LN2 reference had malfunctioned due to a leakage problem. As a result, the radiometer performance was verified radiometrically with two references at +40°C, -40°C during pre-launch system-level environmental tests. The TVAC measurements were made for operational temperatures between 15°C and 25°C, providing an initial estimate of temperature-sensitive coefficients for the instrument calibration.

1.3 Development, Launch and Operation

1.3.1 IceCube Development and Launch

The IceCube development was on an unusually fast schedule (2.5 years) and tight budget, compared to the normal NASA's flight projects. IceCube spacecraft integration and test (I&T) revealed numerous issues with COTS parts and commercial subsystems, for which re-engineering and rework were required for mission reliability and success. Relying on NASA's system engineering approach, the IceCube team was able to identify and minimize the mission-critical risks through vigorous testing on targeted subsystems/components. The final delivered system was a product with medium risks, of which the top two were the mechanisms associated with solar panel deployment and the inhibit switches for battery safety.

The IceCube project started in April 2014 and delivered the system to the CubeSat launch provider (NanoRacks) in December 2016. It was launched to ISS on a rideshare on April 19, 2017, and released from the ISS on May 16 with a delta-V of 1.67 m/s at 45° down-and-backward from the ISS flight, or Vbar, direction. It was contacted immediately during its first pass over the WFF ground station. Successful solar panel deployment and power switch-on were confirmed during the first contact. The first-light observation from the IceCube cloud radiometer was made on June 6. By July 17, there were enough acquired data from IceCube to make the first global 883-GHz cloud map.

The successful IceCube deployment and operations provide a better understanding of CubeSat thermal and dynamic environments, as well as its capability of adapting to, or correcting, the effects from these highly variable conditions. IceCube has encountered some issues during its mission, including largely varying instrument noise, inaccurate orbital Two-Line Elements (TLEs) during downlinks and orbit determination, and data reported in ADACS. The BCT XACT module has been encountering some difficulties staying in FRP mode with frequent incidences of GPS unlocking to star-tracker during science observations. Although the baseline mission for the technology demonstration is 28 days, the actual mission lifetime lasted for ~17 months till October 2019, thanks largely to low solar activity during the current solar minimum.

1.3.2 Concept of Operations (ConOps)

IceCube's flight software operates in three modes: deployment mode (DM), safe hold mode (SH), and science mode (SM). Successfully executed shortly after IceCube was released from ISS, DM represents the startup functionality of spacecraft, beginning with flight computer booting and ending with the spacecraft in SH. SH represents both the minimum functionality necessary to maintain and monitor spacecraft health and the mode in which the spacecraft communicates and responds to ground commands. All troubleshooting activities are conducted in this mode. SH is entered either when ground commands are sent to spacecraft, battery voltage drops below 7.5V or instrument radiator temperatures are outside of survival conditions. SM is the software mode in which spacecraft autonomously measures and records science data either during daytime, or through a pre-defined thermally-controlled instrument operation. The spacecraft must be ground-commanded into SM when in SH. The spacecraft transitions back to SH whenever a ground command is received. It can also transition back to SH autonomously in response to out of range battery voltage or instrument temperature violation. The spacecraft transitions directly from SM to DM if the flight computer automatically performs a soft or hard reset.

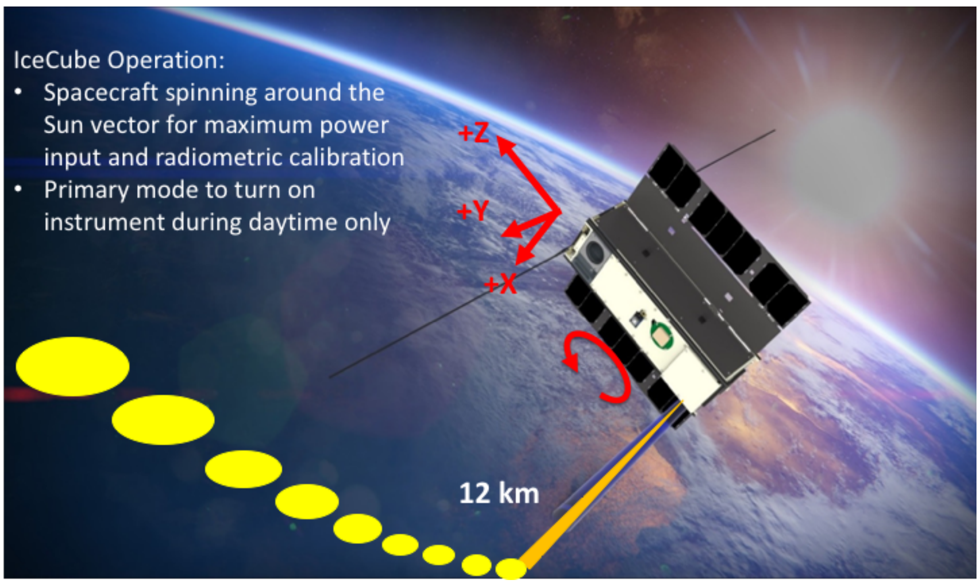

Fig. 1-5. IceCube concept of operation (CONOP). Illustrated is the IceCube's spacecraft spinning around the Sun vector, to maximize solar power input during the spaceflight while allowing periodical views of Earth and cold space for radiometric calibration. The nadir footprint size is ~12km

IceCube ground communications come through the GSFC WFF 18-m UHF dish. Although the IceCube radio is capable of transmitting at a rate of 1.5Mbps, the effective downlink data rate at WFF was ~0.2 Mbps on average during mission operation. There were usually 2-4 daily passes over WFF, producing an average of ~3 contacts per day. Routine operation at WFF was, however, limited to daytime hours on weekdays. The average contact time was ~10 min with a successful rate of 76%, of which ~55% had successful responses to ground-station requests. Because of the IceCube's low data volume, the onboard 4GB memory allowed most of the science data stored onboard to be downlinked on a weekly basis.

IceCube flew in a 52°-inclination orbit similar to ISS, with an initial orbital apogee of 416 km and perigee of 402 km. Each orbit had ~50 min of sunlight time. Because the flight thermal condition and solar power input vary highly with orbital geometry (e.g., beta angle), the initial ConOps was to keep the instrument off, allowing assessment of CubeSat health and establishment of optimal parameters for safe mission operation through both day and night. Two parameters were closely monitored; battery voltage (V_b) where V_b should be greater than 7.5V (vs. normal 8.1V), and payload temperature (T_p) which should be less than 40°C.

IceCube demonstrated spin stabilization using the BCT XACT system. It has been spun at various rates between 0.2 and 3.3 degrees per second (dps). During the early period of the mission, the FRP mode with a spin rate of 1.2 dps was employed. At this rate, the star-tracker was able to acquire good navigation data while the spacecraft spun. However, there has been an issue in the FRP operation to keep GPS locked to the star-tracker continuously. In the event of unlocking, a reset command has to be sent to the spacecraft, to re-initiate the FRP operation. Since unlocking events occurred frequently, the FRP operation reset was abandoned during operation after October 2017, leaving most of the observations from the SP mode in the recent months.

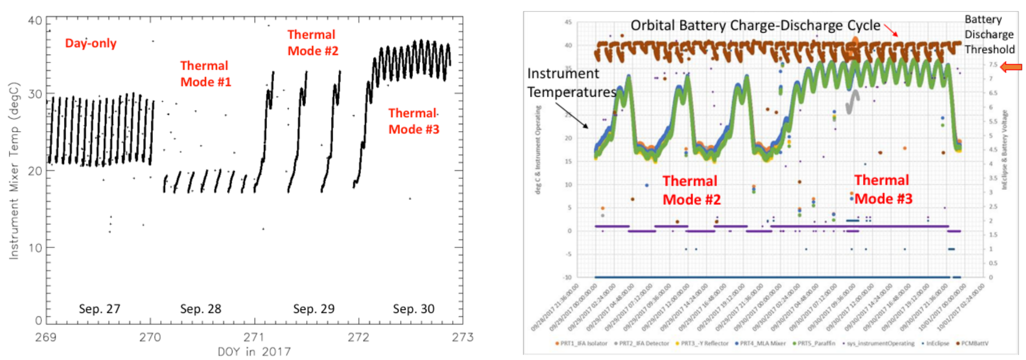

(a) (b)

Fig. 1-6. (a) IceCube T_p from four operational experiments with the instrument powered on and off at different time intervals. The thermal-mode #3 is the 24/7 science operation when T_p reached an equilibrium of 34-38°C. (b) Detailed temperature and battery voltage variations during the 24/7 operation, showing that the voltage stayed above the 7.5V threshold and all instrument temperatures plateaued at 38°C. The thermal test #3 confirms that the 40-Whr battery can support full-day operation of the 5.6W payload.

During daytime the spacecraft spins around the Sun vector (-Y axis) to produce maximum solar power while allowing the radiometer to be calibrated periodically [Fig. 1-5]. This operation is called the daytime-only science mode (DO-SM), in which BCT XACT spins around -Y axis at a rate of 1.0 dps in the SP mode or around +Z axis at 1.2 dps in the FRP mode. The XACT performs attitude determination autonomously. The Kalman attitude filter operates constantly in the background (even in the SP mode). The algorithm would not return a valid attitude until a valid attitude measurement has been obtained from the star tracker. If the tracker ceases to provide valid attitude measurements, the onboard attitude remains valid for a table-valued duration (nominally 1 hour) as long as the inertial measurement unit (IMU) measurements are available to propagate it. The bias stability of the XACT IMU is ~3 degrees over an hour.

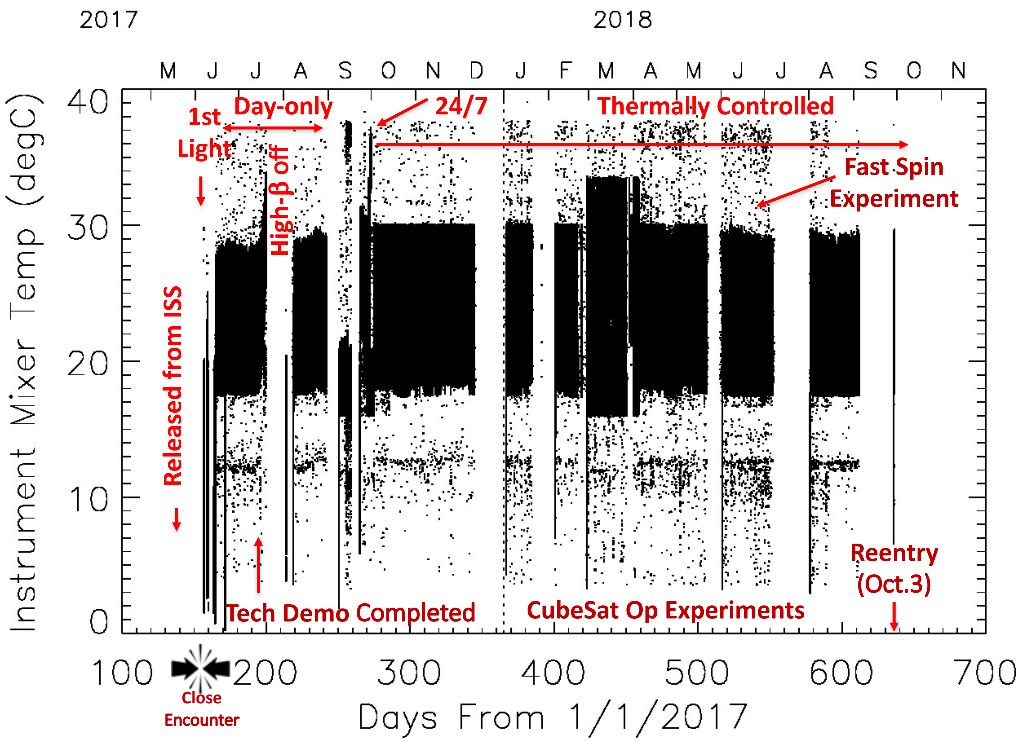

Fig. 1-7. IceCube T_p variations during different operational modes/experiments since launch. IceCube had a close encounter but avoided the collision with another CubeSat shortly after released from ISS. The coldest temperature is ~2°C when the instrument was powered off for a long period of time. The warmest temperature (~38°C) occurred when the cloud radiometer was powered on continuously for 24 hours. The operation was thermally controlled after Oct 2017 with T_p capped at 30°C.

At night IceCube relies on its onboard magnetometer to align the spacecraft's +Z axis along the geomagnetic field. The spacecraft spins around the +Z axis at a rate of ~1.5 dps at night. The battery discharges gradually after the spacecraft enters eclipse, but need to maintain an output voltage above 7.5V in order to avoid over-discharging. During the initial operation a conservative approach was adopted by powering on the instrument only during daytime, to assure the battery adequately charged all the time during the 28-day technology demonstration period (i.e., primary mission).

On September 30, 2017 IceCube successfully conducted a 24/7 experiment for the full-power cloud radiometer operation. Using its double-sided solar panels and 40 Whr battery, the CubeSat can support a 5.6 W payload for full-time operation. With this mode, basically, the 883-GHz radiometer is left on all the time, which produces the most stressful operation on the spacecraft battery. It was first used on June 8 for two consecutive orbits. Since the operation time was short, the instrument did not reach its thermal equilibrium and the battery stress was not long enough to verify its capability. It was tested again on September 30 for approximately one day when the instrument reached a thermal equilibrium of ~38°C [Fig. 1-6], which is still below the limit (40°C) for safe instrument operation. In this experiment the battery voltage never dropped below 7.5V, confirming that the 40 Whr battery can support the 24/7 operation of the 5.6-W payload. Because the 883-GHz radiometer becomes much noisier above 35°C for cloud observations, 24/7 operation was modified to keep the instrument on only below 30°C. This operation is called thermally-controlled science mode (TC-SM), such that the instrument is automatically powered off when T_p reaches 30°C and powered back on when T_p drops to 18°C. The TC-SM operation is a fully autonomous mode and has been employed since October 2017.

The spacecraft and instrument thermal environments play an important role in operating the 883-GHz cloud radiometer. As shown in Fig. 1-7 the DO-SM operation yielded a relatively stable orbit-to-orbit thermal range (18°C -29°C) for T_p when the beta angle is normal. Note that the time in eclipse, when the spacecraft cools, gets shorter as beta angle increases, and can go to zero (no eclipses) as beta angle approaches 90°. During a high beta-angle period (e.g., July 20 – Aug 10, 2017), T_p rose quickly and the instrument was powered off. During the DO-SM operation, the instrument was on for ~58% time of the orbit period. A drawback of the DO-SM operation is that it requires the special care needed to monitor the instrument temperature in the high beta-angle condition. Therefore, a thermal-controlled operation was developed and implemented to achieve fully autonomous operation. Fig. 1-7 also reveals the days when the cloud radiometer was re-started from a power-off. After the instrument is powered off, its temperature usually drops below 10°C, indicating the instrument turn-on days.

1.4 Technology Validation

The IceCube 883-GHz cloud radiometer had first light on June 6, 2017 for two orbits. The data acquired by the commercial radiometer showed good sensitivity to Earth and space scenes [Fig. 1-8], as expected from the CubeSat programmed to spin around the Sun vector during daytime. Cloud scattering signatures can be readily seen in the raw count data as reduction from the background Earth-view counts.

Validation of the commercial 883-GHz receiver technology requires verification of the instrument's sensitivity and demonstration of a calibratable system in realistic spaceflight environments (e.g., thermal variations and radiation). While Fig. 1-8 provides the sensitivity verification (in terms of measurement counts) at a specific operation temperature, the sensitivity variation with T_p needs to be characterized. To achieve this goal, we estimate the instrument sensitivity (i.e., gain) as a function of T_p, using the modeled Earth clear-sky radiance and the cold space radiance as the two reference points. The clear-sky radiances are calculated by the radiative transfer model used for Microwave Limb Sounder (MLS) observations [Wu et al., 2006], which has accuracy of 5K. The modeled radiances are sufficient to provide the gain/sensitivity evaluation. The model requires input parameters for atmospheric pressure, temperature, water vapor, and ozone profiles that are obtained from the daily MERRA-2 reanalysis [Bosilovich et al., 2015].

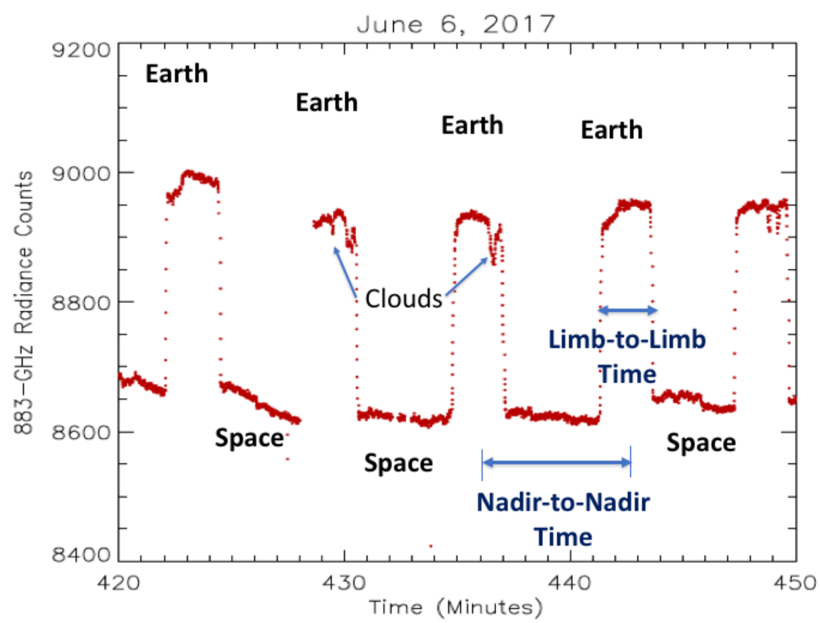

Fig. 1-8. The first-light 883-GHz measurements on June 6, 2017, showing the radiance counts from spinning CubeSat during Earth and cold space views. Cloud scattering is clearly evident in some of the Earth's views. Each measurement has a 0.52-s integration time. Limb-to-Limb (LLT) and Nadir-to-Nadir time (NNT) intervals can be used to evaluate the CubeSat spin rate.

1.4.1 CubeSat Spin and Attitude Control

Because IceCube relies on the spinning spacecraft for the Earth and space views, the pointing accuracy becomes important for registering the measurement geolocation. The pointing knowledge depends on how well the sensors are capable of tracking the Sun or the magnetic field and by how accurately spacecraft can spin at the rate specified. As illustrated by Fig. 1-5, IceCube spins around the Sun vector (-Y axis) during day. The spin rate depends on operation mode: -1 dps (SP mode) or -1.2 dps (FRP mode). Several spin anomalies occurred during daytime, when it spun at a very slow rate (0.2-0.3 dps). The observations from these slow spins make the radiometer difficult to calibrate because of fewer space views. At night IceCube spins around the +Z axis along the magnetic field. The nighttime spin rate varies between +1 and +2 dps. In both day and night spins, the cloud radiometer FOV (+X axis) is orthogonal to the spin axis.

The spin requirement imposed by IceCube was the first application of such kind with the BCT XACT. Challenged by the dual tasks for XACT, the ADACS system has to maintain both (slow) 3-axis attitude control and (fast) spin operation. IceCube had trouble with the star tracker not reacquiring after being occulted. The BCT XACT would default itself into SP mode if the missed star tracker acquisition went longer than 60 minutes. The default from FRP to SP mode did not cause the spacecraft to drop out of science mode, except to yield a different spin rate (-1.2 dps vs -1 dps). It requires a ground command to set XACT back to FRP mode, but the frequent occurrence of XACT default to SP mode had led to the later IceCube operation mostly in SP mode.

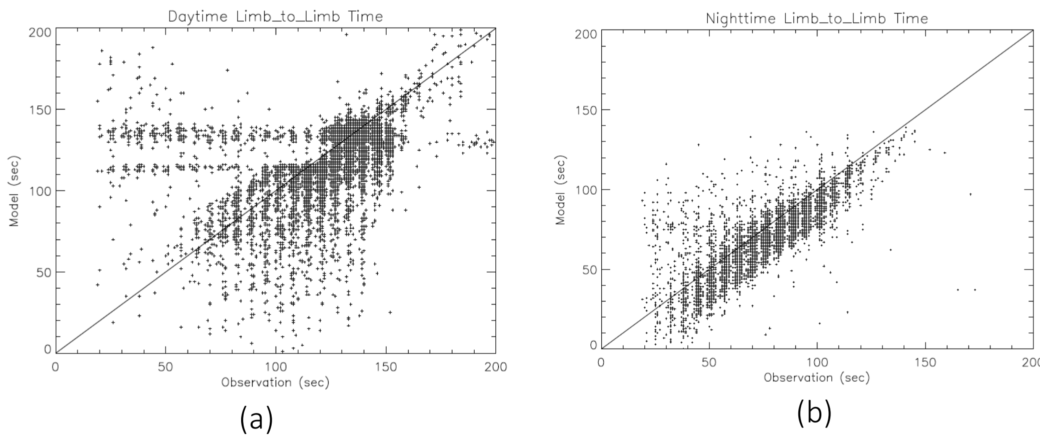

Fig. 1-9. Modeled and observed LLTs from (a) daytime and (b) nighttime data. The horizontal bands in the daytime data are the bad situations where the derived LLTs are unreliable due to data gaps.

In SP mode the CSS used by IceCube is expected to have pointing accuracy no better than ~5°. The nighttime pointing is not expected to be better than daytime pointing, because the magnetic field is a weak source for navigation. Verification of IceCube's spin rate in SP mode became a critical task to geo-register the 883-GHz measurements and to calculate the associated clear-sky radiance. Discrepancies between the reported and estimated spin rates were found during the early IceCube operation, showing that the observed limb-to-limb time (LLT) and nadir-to-nadir time (NNT), as defined in Fig. 1-8, were significantly different from the values calculated. The 883-GHz cloud radiometer on IceCube has a narrow (1.8°) FOV, and its limb measurements can be used to determine accurately where the instrument's FOV is pointing relative to its sub-nadir point in a scan. From the spacecraft TLE orbital parameters, the sub-nadir location is relatively well known. Thus, the rest of scan positions can be determined from the spin rate if the reported value is accurate.

Both LLT and NNT data were used to validate the accuracy of the spacecraft spin rate reported in telemetry. As seen in Fig. 1-8, the count measurements exhibit a sharp transition at limb, from which the LLT and NNT can be determined as accurately as ~1 s. If the spacecraft spins faster than the reported spin rate, the observed LLT and NNT would be shorter than the calculated. The difference between the measured and calculated LLTs and NNTs indicate possible errors in the spin rate and the sun-pointing operation.

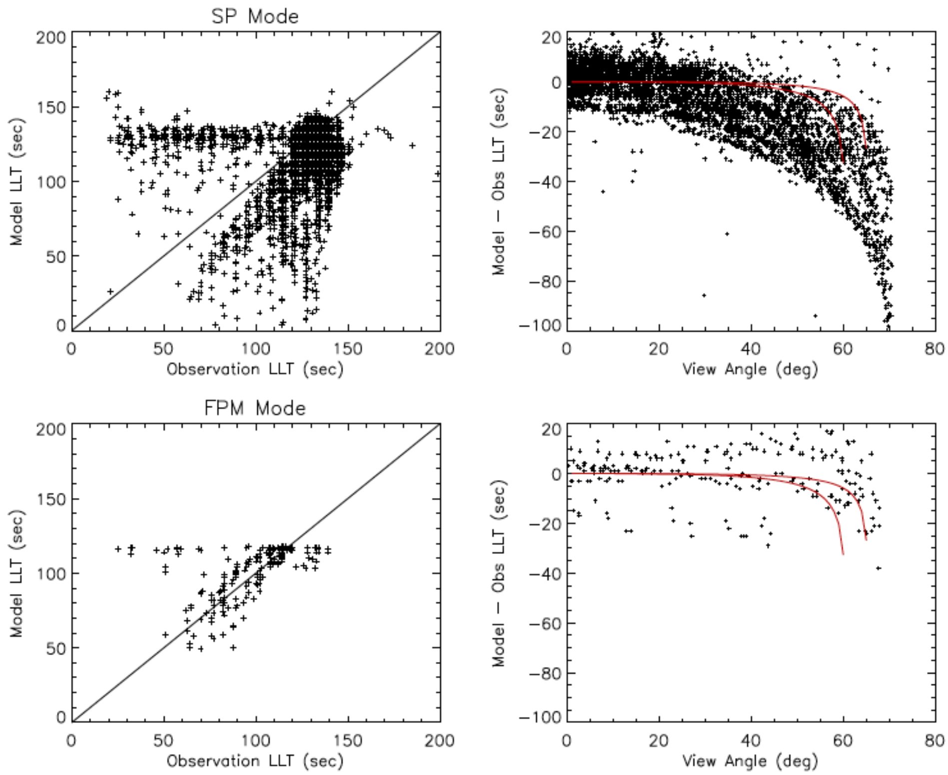

Fig. 1-10. Daytime LLTs from SP mode (top panels) and FRP (bottom panels). Correlations between observed and calculated LLTs are in the left panels, whereas their differences are plotted in the right panels as a function of the minimum view angle from nadir of each scan. Significant scaling biases are found in the LLT under the SP mode. The red lines indicate the LLT differences that would come from a CSS Sun-pointing error of 5° and 10°.

Fig. 1-9 exhibits the correlation of observed and calculated LLTs for day and night observations. Larger scatters in the daytime than nighttime data indicate uncertainty in the reported spin rate, showing a slight low bias in the calculated LLTs. The low bias is more pronounced in the nighttime data, implying that the reported spin rates were faster than the actual rates. By dividing the daytime LLTs into the SP and FRP modes [Fig. 1-10], it becomes clearer that the bias is mostly associated with the SP mode in which the Sun pointing relies on CSS and the ADACS has no inputs from GPS and star-trackers for fine pointing controls. As indicated by the red lines in Fig. 1-10, the CSS Sun-pointing error could hardly explain the differences between the observed and calculated LLTs in the SP operation. A systematic error likely exists in the reported spin rate in SP mode, which tends to increase with the scan view angle. The scan view angle is the minimum angle from nadir in each scan, which is reversely related to solar zenith angle (SZA). Since most of the IceCube data were acquired under the SP mode, we excluded the data of the scan view angle > 50° in subsequent data processing, to minimize the geo-registration error induced by the spin rate bias.

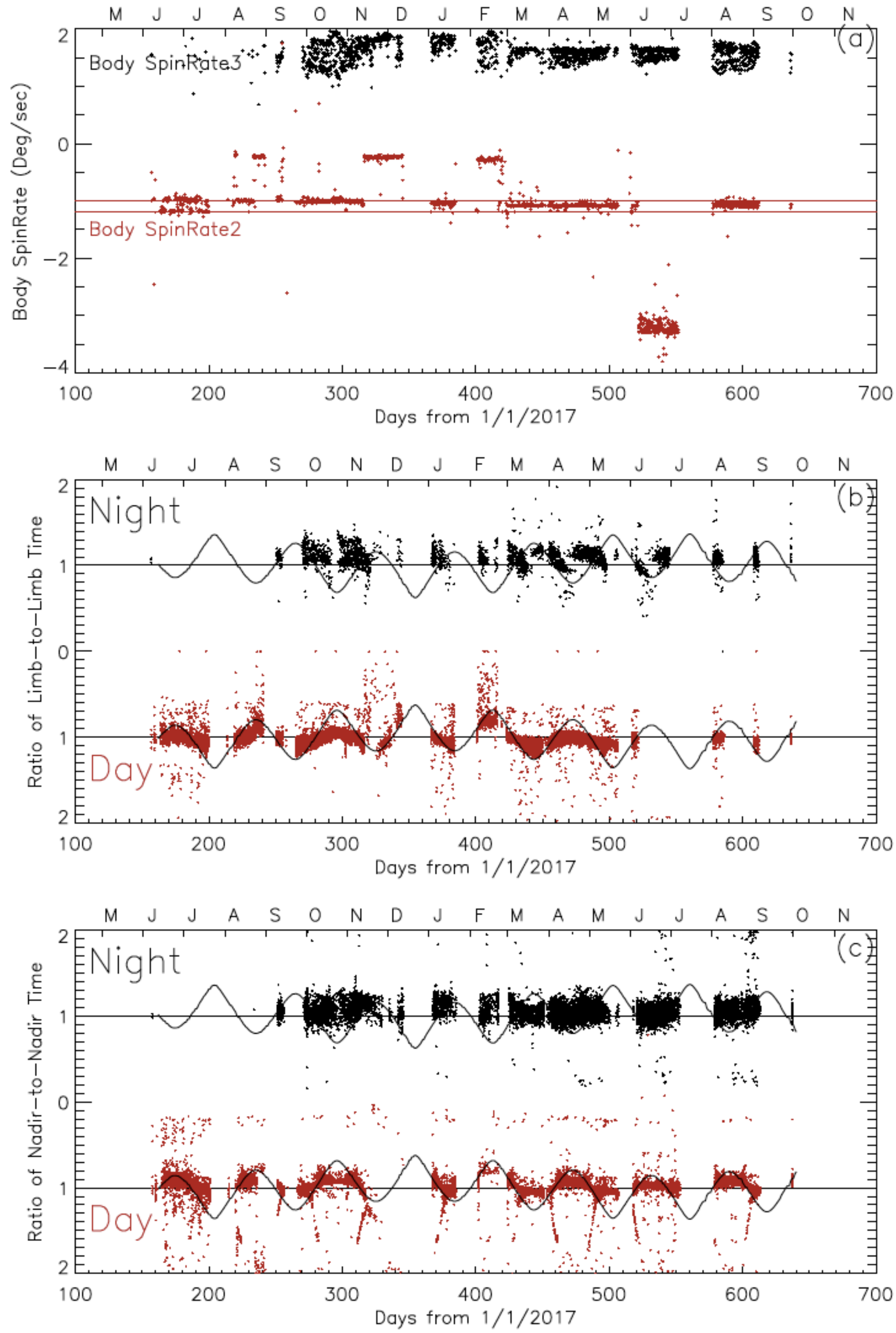

Fig. 1-11. Time series of (a) daytime (red) and nighttime (black) spin rates, (b) ratio of observed over calculated LLTs, and (c) ratio of observed over calculated NNTs. The curved lines in (b) and (c) indicate the beta angle variations. IceCube

spins around the Sun vector (-Y) during day (body rate-2) and around the magnetic field during night (+Z, or body rate-3), as defined in Fig. 1-5.

To monitor the spin rate bias, we ratio the observed and calculated LLTs and NNTs and plot it in Fig. 1-11 for both day and night. There is a beta-angle dependent variation in the daytime LLT and NNT ratios, which is consistent with the view-angle/SZA dependence seen in Fig. 1-10. The nighttime LLT and NNT ratios show little beta-angle dependence and are consistently greater than 1, confirming that the reported spin rates were faster than the actual rate by 10-20%. The nighttime spin rates vary typically between 1.3 and 1.8 dps around the +Z axis. The larger spread of the nighttime spin rates is partly because magnetic field is a weaker source for navigation. A fast spin experiment was conducted in June 2018 during which the spacecraft was commanded to spin at 3.3 deg/sec during the daytime orbit [Fig. 1-11a]. The experiment was successful with similar performance to the low-rate operation and produced useful science data.

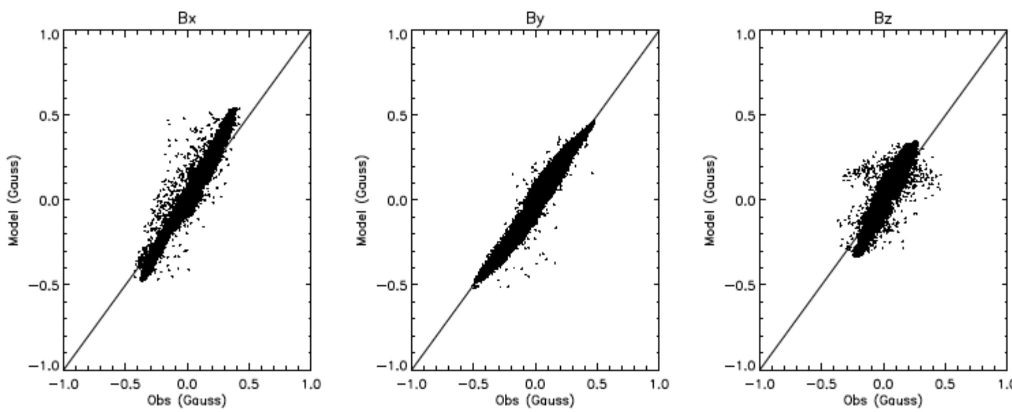

Fig. 1-12. Observed and modeled magnetic field component projected onto the spacecraft coordinate (X, Y, Z) as in Fig. 1-5. Scaling errors are evident in the Bx and Bz components.

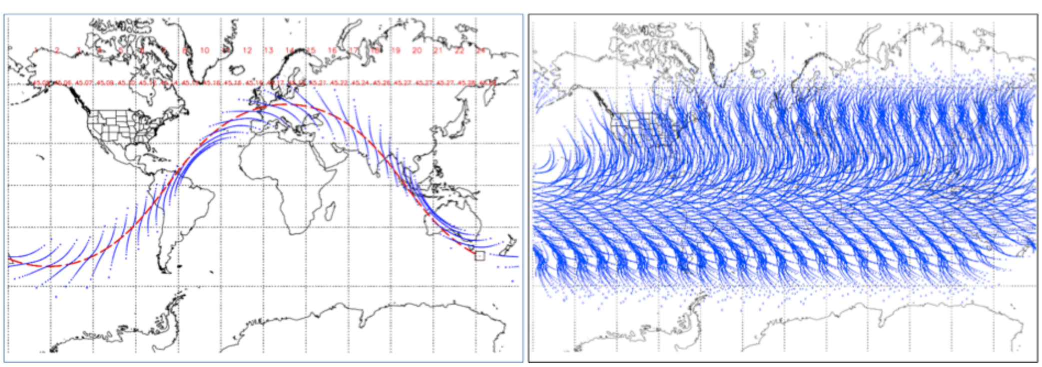

Fig. 1-13. IceCube daily (left) and weekly (right) sampling simulated for the DO-SM operation.

The three-axis magnetometer embedded in BCT XACT is critical to momentum control in SP mode. Its output is available as the "observed" magnetic field in telemetry. In contrast, in FRP mode the momentum field is deduced from onboard time and ephemeris using a high-precision model of Earth's magnetic field. Although XACT provides the "modeled" magnetic field in telemetry, we used an offline International Geomagnetic Reference Field (IGRF) [Thébault, et al., 2015] to compare the observed magnetic field. The comparison of observed vs. modeled magnetic field is an indicator of magnetometer health and performance. Fig. 1-12 shows that the observed and modeled magnetic fields agree well in the Y component. The magnetometer precision helps to identify a significant scaling error in the X and Z components, which was not readily seen in the Miniature X-ray Solar Spectrometer-1 (MinXSS-1) data [Mason et al., 2017]. MinXSS-1, a 3U CubeSat, also employed the BCT XACT. The scaling error in IceCube magnetometer measurements is similar in both SP and FRP modes when plotted separately, suggesting that it is intrinsic to the magnetometer, which could affect the accuracy of IceCube attitude determination at night.

IceCube footprints on Earth are irregular, because of the spins around Sun and magnetic field. The sampling varies from cross-track-like scans in low-beta twilight to along-track scans in high-beta twilight. As illustrated in Fig. 1-13, during the Sun-pointing DO-SM operation, the sampling of IceCube measurements is neither cross-track nor along-track, but can produce a wide swath coverage. The weekly sampling can produce a good global coverage in longitude if all measurements are used. In the routine IceCube data processing, the geo-registration is performed on a spin-by-spin basis, using the spin rate provided by the spacecraft and the sub-nadir time and location calculated from the orbital TLE parameters. The middle time of LLT is where the cloud radiometer points at the sub-nadir. Since the IceCube orbit is well determined, this sub-nadir location is relatively well known. Using the spacecraft's spin rate and the sub-nadir location, we can determine the pointing angle and location within each spin to ~10% accuracy. The pointing angles far away from the sub-nadir are likely associated with a higher uncertainty due to an accumulated error from the spin rate bias. Therefore, the measurements with a view angle greater than 50° from the sub-nadir are generally excluded for cloud observations, while a 30° threshold would yield better quality control but with less coverage.

1.4.2 Calibration of Space-View Count

The IceCube 883-GHz cloud radiometer is operated differently from most of MW radiometers in two ways: 1) power-cycling MLA at 50% duty cycle while the instrument is on, and 2) power-cycling the instrument on an orbital basis. In essence, it is a free-running radiometer without onboard calibration targets. In contrast, conventional MW radiometers operate with MLA-on continuously once the instrument is powered, which allows MLA to reach an equilibrium both thermally and electrically. For the IceCube radiometer, MLA is switched on and off every 20 ms. Thus, the receiver system never reaches a fully equilibrium state before MLA is switched off. The IceCube radiometer employs this special design to study and explore new ways for radiometric calibration.

The radiometer system produces radiance (T_b) and count (C) measurements that can be expressed mathematically by

$$C(T_p) = G(T_p) \cdot T_b + C_0(t, T_p) \qquad \text{(Eq.1)}$$

where the background count (C_0) and gain (G) may vary with time (t) and T_p. Characterizing $C_0(t, T_p)$ requires frequent cold space measurements, which comes from the spacecraft spinning. Because IceCube was power-cycling on every orbit, the number of space views was limited and broken in time series.

One of the challenges in IceCube calibration is to model the time- and T_p-dependent variations of space counts, $C_0(t, T_p)$ in Eq.1. When the radiometer is powered on after being off for a while, T_p is usually low but can rise rapidly by 10°C-15°C [Fig. 1-7]. As a result, there exist significant variations in the background count C_0. Fig. 1-14 shows that C_0 can vary by 2500 in an orbit while the Earth-space count differences (i.e., Earth atmospheric signals) are only ~300.

While Antenna (*Ant*) and Reference (*Ref*) C_0 measurements may be a complicated function of T_p, the background C_0 in the *Ant-Ref* difference appears to depend simply on T_p [Fig. 1-14]. At low T_p when the instrument is just powered on, C_0 usually rises with T_p (a start-up effect), likely due to a delayed thermal response in the radiometer backend. After ~5 min from the power-on, C_0 begins to decrease with T_p near linearly. Although it is difficult to fit the T_p dependence for *Ant* and *Ref* C_0 counts, it is feasible to fit an empirical function to the *Ant-Ref* difference as a function of T_p. In other words, the reference state (*Ref*) from the 50% MLA duty-cycling experiment helps to remove some of the complex thermal responses in C_0. Hence, we use the *Ant-Ref* count difference hereafter for IceCube radiometric calibration. All variables in Eq.1 represent *Ant-Ref* counts.

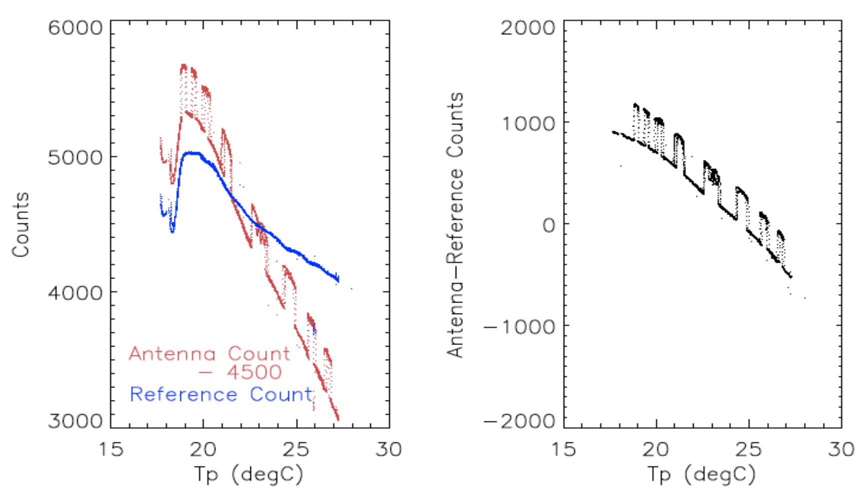

Fig. 1-14. (a) Tp-dependence of Antenna (Ant) and Reference (Ref) counts from two orbits of data on July 10, 2017. (b) Tp-dependence of Ant-Ref count difference. The raw Ant and Ref count time series in (a) contain complex dependence on Tp, showing a start-up effect when the instrument is powered at low Tp. The start-up effect is less pronounced in the Ant-Ref count difference, making it calibratable using Tp-dependent functions.

Fig. 1-15 illustrate the steps needed to model orbital variations of the background space count C_0 as a function of T_p and time t, namely $C_0(t, T_p)$. An ideal calibration would yield zero residuals between the modeled and modeled $C_0(t, T_p)$. Nevertheless, the empirical model $C_0(t, T_p)$ needs to count for a large degree of variability as well as operational anomalies (e.g., data gaps). The algorithm assumes that $C_0(t, T_p)$ varies slowly within an orbit such that these variations could be modeled/fitted with polynomial and sinusoidal functions.

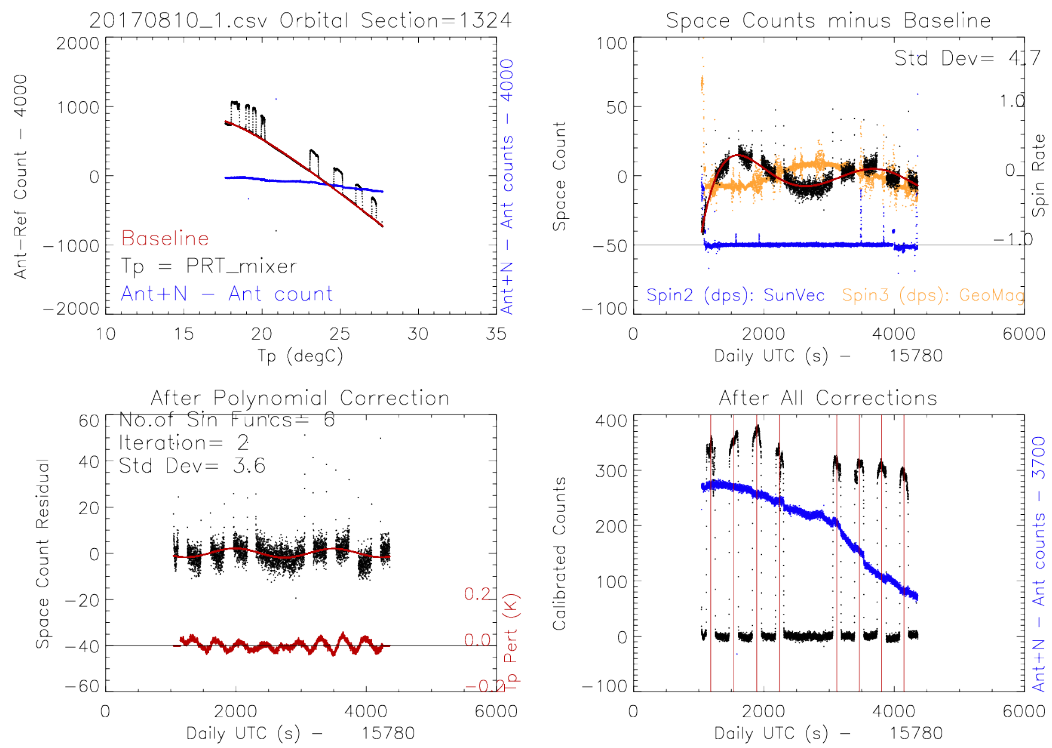

Fig. 1-15. A 3-step fitting algorithm with empirical functions to model the space count variations on an orbit-by-orbit basis. The fitting is able to track space count variations (~2000 counts over a 10°C variation in T_p) precisely, such that the standard deviation from the fitting residual is < 4 in count. The modeled space count function is applied to the Earth-view count measurements, to remove T_p dependent background variations $C_0(t, T_p)$ in Eq.1.

The fitting procedure for the background $C_0(t, T_p)$ calibration algorithm is described as follows. In the first step [Fig. 1-15a], a 2^{nd}-order polynomial is fitted to the count variation as a function of T_p. This fit removes most of the large variations due to T_p and reduces the C_0 residuals to ±50. In the second step [Fig. 1-15b], the C_0 residuals are fitted to another multi-order polynomial but with respect to time t, to take care of time-dependent C_0 variations. The 2^{nd} fit helps to bring the C_0 residuals down to ±20. In the third step [Fig. 1-15c], the remaining C_0 residuals are fitted to a multi-periodicity sinusoidal function to remove periodic variations in C_0 that may come from the spinning operation. As shown in the time series [Fig. 1-15c], there exists a small T_p oscillation that synchronizes with the CubeSat spinning cycle, which has been pronounced only during day, not much during night. The lack of spin-cycle variability at night implies that Earth radiation had little impacts on the spacecraft thermal fluctuation during its spin. In any case, this spin-like C_0 oscillations can be removed by fitting the residuals to sinusoidal functions correction, yielding a standard deviation of <4 in the final C_0 residuals. The combined function from the fittings to the orbital data, $C_0(t, T_p)$, provides an empirical background correction for this orbit. The difference between the raw count $C(T_p)$ and $C_0(t, T_p)$ renders the calibrated counts with the background removed [Fig. 1-15d]. As a result, the space-view counts are approximately zero and the Earth-view counts are ~300. The Earth-view counts are further used for radiometer gain evaluation and cloud detection.

1.4.3 The 883-GHz Radiometer Gain

The IceCube 883-GHz radiometer was calibrated twice on the ground: one during the instrument thermal vacuum (TVAC) test over a narrow temperature range of 19.8°C-21.5°C and the other during the system TVAC test when it was integrated onto CubeSat over a temperature range of 18°C-24°C. The gain measured during the instrument TVAC used two targets at ~100K and ~300K. The gain measured during the system TVAC test was from the targets at ±40°C. The main objective of the system TVAC test at WFF was to verify CubeSat deployment mechanisms, as well as other spacecraft and payload functionalities. A 5-day, 4-cycle test was conducted for the system TVAC. The gain from the instrument TVAC was measured as 2.37 counts/K at 20°C, but it dropped surprisingly to ~1.1 counts/K at 20°C during the system TVAC [Fig. 1-16a].

This unexpected gain drop was speculated as a result of some debris falling into the receiver's feedhorn during the system I&T, causing the gain degradation. The instrument did not have any major modification in between, and its gain was verified before and after a vibration test prior to the integration onto the CubeSat. It is plausible for some debris went into the 883-GHz frontend horn because it had been exposed all the time during the system I&T period. Such debris could be very tiny and difficult to identify from visual inspection. For future CubeSat I&T, MW feedhorns need to be protected carefully with a cover or the equivalent. Despite the gain degradation, as a technology demonstration experiment, IceCube was able to calibrate 883-GHz radiometer through frequent space views.

Using the modeled Earth clear-sky radiances, the 883-GHz receiver gain is further validated during spaceflight over a large temperature range (4°C-38°C) [Fig. 1-16]. The IceCube clear-sky radiances from the Earth's atmosphere are modeled using the same radiative transfer model as for MLS [Wu et al., 2006], except for 883 GHz. The instrument gain is computed as the ratio of clear-sky count measurements over the modeled radiances, since the calibrated cold-space count and radiance are zero. As expected, the radiometer gain is a function of T_p [Fig. 1-16a] and degrades with time [Fig. 1-16b]. The T_p-dependence of gain variation is similar to the prelaunch measurements, except to shift up by ~0.4 counts/K. Again, this gain shift is consistent with the debris-in-feedhorn hypothesis that the launch and thermal expansion could all make the gain change.

Gain degradation of VDI's 883-GHz receiver was found and characterized through IceCube demonstration [Fig. 1-16b], one of the benefits of long-term operation. It highlights the unique value of spaceflight demonstration for future spaceborne technologies that would not be achievable in balloon-borne or ground-based tests. Since the VDI's 883-GHz receiver on IceCube was designed to operate at 20°±2°C, it is not completely surprising that the instrument gain starts to degrade very little at 20°C but more substantially at temperatures warmer than 23°C. The gain degradation is likely to occur within the receiver frontend such as MLA, as a common degradation in other MW sensors. It is unlikely due to the theorized debris-in-feedhorn because the degradation from debris would occur abruptly as on June 19, 2017 and would induce degradation at all temperatures.

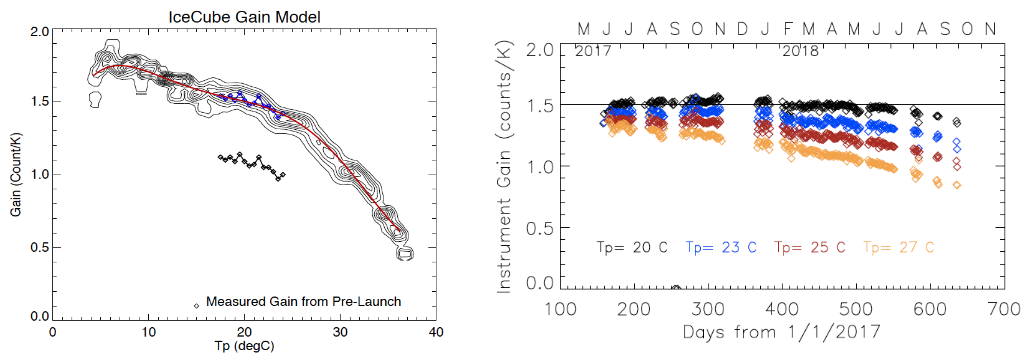

(a) (b)

Fig. 1-16. (a) T_p-dependent instrument gain model (red line) for June-August 2017. The gain is estimated from the modeled clear-sky radiances. The prelaunch gain measurements from the system TVAC are the black symbols. They are shifted up by ~0.4 counts/K to match the in-flight gain estimate. (b) Gain stability of the IceCube 883-GHz radiometer at T_p=20, 23, 25, and 27°C, showing steady degradation at warmer temperatures. The radiometer was designed to operate at temperatures of 20± 2°C, at which only small degradation is found in gain over the first 13-month operation period. The degradation at 20°C became significant in the final three months of operation.

1.4.4 Noise Source Experiment

The IceCube 883-GHz radiometer carries a noise source experiment for IF calibration with noise injection and LO power modulation. As shown in Fig. 1-3, at MLA on and off states, the noise source can be switched on and off, namely *Ant+Noise* and *Ref+Noise*, providing four outputs: $C_{Ant+Noise}$, C_{Ant}, $C_{Ref+Noise}$ and C_{Ref} . These measurements provide valuable diagnostics of the partition between the frontend and the backend contributions to the system's radiometric noise. The count differences, $C_{Ant+Noise}$ - C_{Ant} and $C_{Ref+Noise}$ – C_{Ref}, offer different aspects of the noise diode contributions: one involved with the instrument frontend and the backend, the other involved only with the backend.

Stability of noise diodes and their long-term operational uses have been an interesting research topic. As seen in Fig. 1-17, the IceCube's noise diode has not been a constant source over the period of its 15-month operation. The measured noise source contributions, $C_{Ant+Noise}$ - C_{Ant} and $C_{Ref+Noise}$ – C_{Ref}, are a strong function of instrument temperature. Both exhibit an increase trend with a steeper slope in the early period of the mission, but the rate of change became nearly linear after four months. It is worth noting that the two noise count measurements maintain roughly the same difference at 20°C but this separation becomes narrower at 25°C, which could be related to the gain degradation at a warmer temperature. Another interesting feature in the $C_{Ant+Noise}$ - C_{Ant} time series is the jump on day 170 (June 19, 2017), which was absent in in $C_{Ref+Noise}$ – C_{Ref}, suggesting that the abrupt change likely occurred in the frontend as speculated from the theorized debris-in-feedhorn. This abrupt change on day170 is also seen evident in the gain time series [Fig. 1-16b].

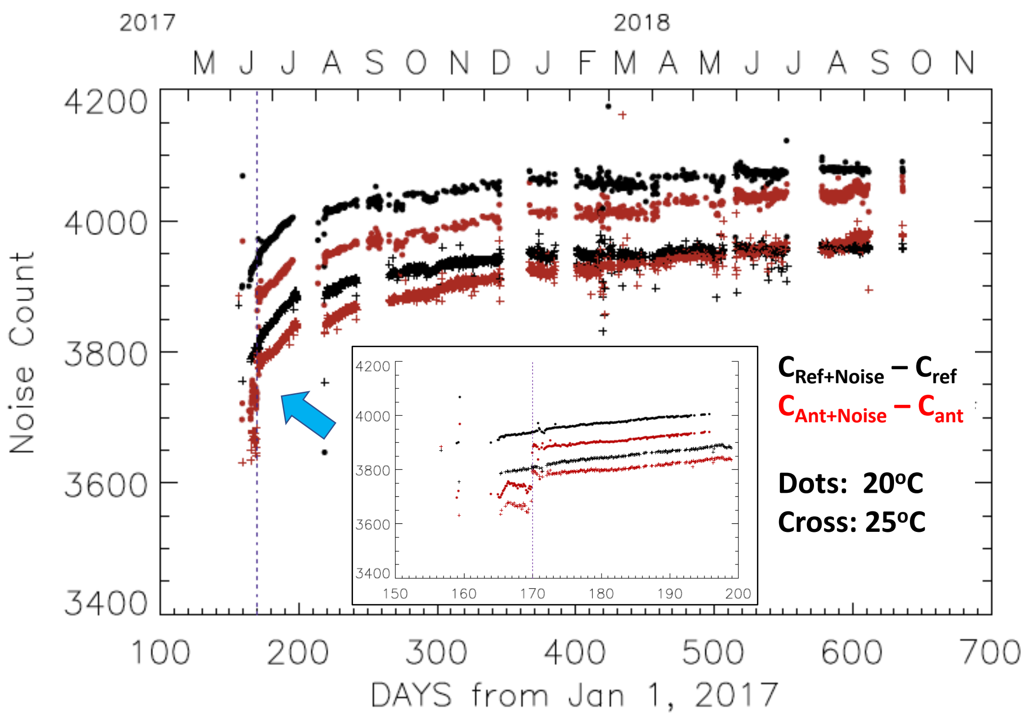

Fig. 1-17. Time series of the noise source power as measured by $C_{Ant+Noise}$ - C_{Ant} and $C_{Ref+Noise}$ – C_{Ref} at 20°C and 25°C. The dashed line indicates the sudden shift on June 19, 2017 in $C_{Ant+Noise}$ - C_{Ant}, but not in $C_{Ref+Noise}$ – C_{Ref}. The abrupt change is also found in the C_{Ant}-T_p relationship and in the instrument gain.

1.5 Cloud Observations

As with other nadir/slant/limb viewing microwave sensors [e.g., Zhao and Weng, 2002; Wu et al., 2005; Wu et al., 2008; Eriksson et al., 2008; Gong and Wu, 2014], ice cloud detection requires significant contrast between the cloudy- and clear-sky radiances. This difference is also called cloud-induced radiance

(*Tcir*). We compute the 883-GHz *Tcir* from the observed radiance (T_b) calibrated from Eq.1 and the clear-sky radiance (T_0) from the radiative transfer model as described above, i.e.,

$$Tcir = T_b - T_0 \quad \text{(Eq.2)}$$

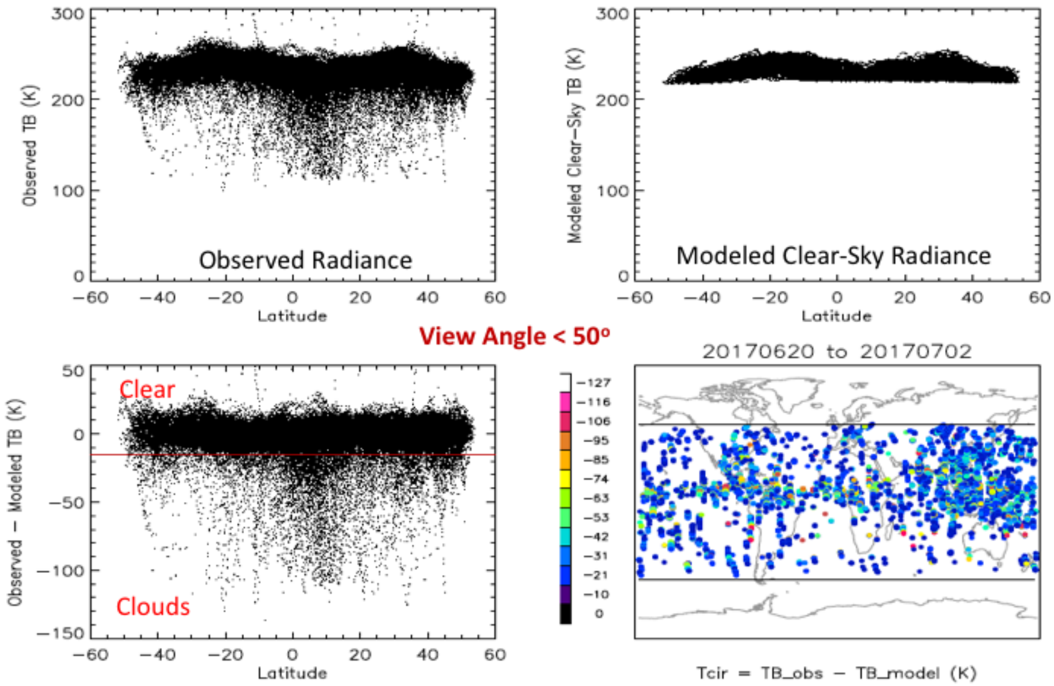

Fig. 1-18. Cloud detection with IceCube 883-GHz radiances. The top panels show the observed and modeled radiances, from which Tcir are computed as their difference. Only data with view angle < 50° are used. The Tcir below the threshold of -15K (red line) indicate significant cloud scattering. The distribution of flagged Tcir is shown on the right-bottom panel. IceCube has a latitude coverage between 52°S-52°N, similar to the ISS orbit.

Table 1-3. Saturation Height of pIWP for Selected MW Channels

Sensors	Avg. T_b (K)	Atmos. T (K)	Est. Height (km)
IceCube 883 GHz	220	240	~8
MLS 118 GHz	220	222	~10.5
MLS 190 GHz	242	247	~7
MLS 240 GHz	240	246	~7
MLS 640 GHz	205	220	~10.7

A threshold of -15 K, approximately 3σ of the *Tcir* variability in clear sky, is applied to IceCube *Tcir* to flag the significant radiance depression due to cloud scattering [Fig. 1-18]. The 3σ clear-sky *Tcir* variability was suggested as a reliable threshold to minimize false cloud detection [Wu et al., 2008]. In spaceborne cloud remote sensing, *Tcir* variability is often dominated by systematic errors associated with the modeled clear-sky radiance T_b. In the IceCube case, the radiance measurement error is comparable with T_b errors, because of the challenges of radiometric calibration as discussed in section 1.4.2.

The detected *Tcir* are further converted to *pIWP* using a modeled *pIWP-Tcir* relation that can be derived from the radiative transfer model [Wu et al., 2006], where *pIWP* is a partial column of cloud *IWP*. Wu et al. [2009) compared the cloud ice observed by passive MW sensors with CloudSat measurements, and concluded that none of the passive sensors from space can measure the entire column of cloud ice, especially in the presence of thick-and-dense clouds. Strong extinction from clear-sky absorption and cloud scattering prevents the radiation from penetrating deep into these clouds, causing saturation in cloud ice sensitivity. It is this saturation that yields a partial column *pIWP* and must be taken into account when comparing cloud ice measurements from different sensors.

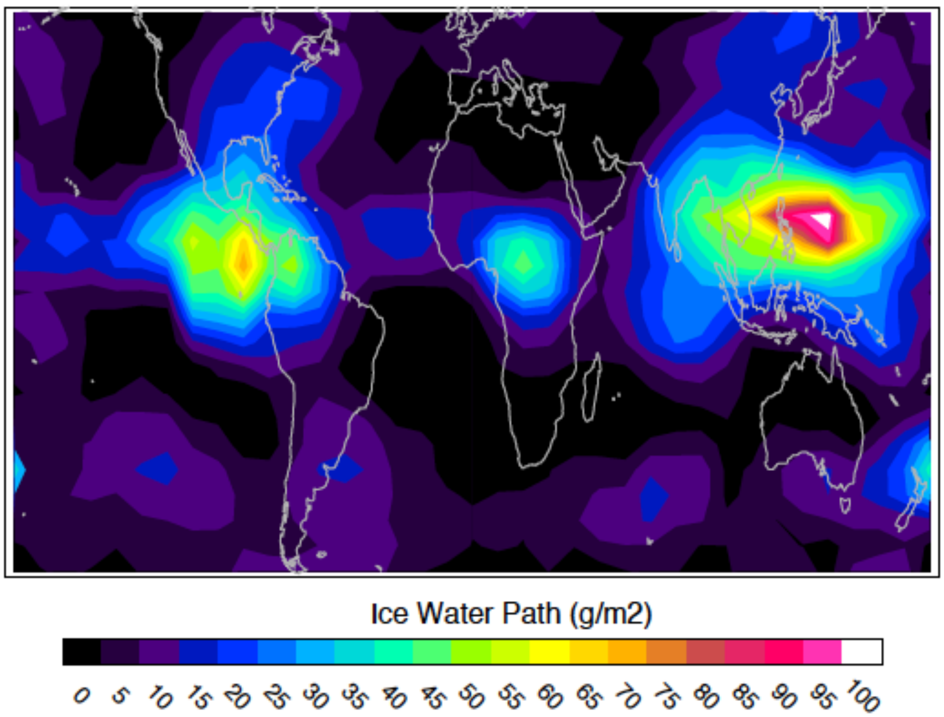

Fig. 1-19. IceCube 883-GHz cloud pIWP map for July-September 2017 at latitudes between 52°S-52°N. A longitude-latitude grid of 10°x5° is used for computing the map. As in Fig. 15, Tcir is discriminated with the -15K threshold, and only measurements with T_p < 30°C and view angle < 50° from nadir are used. Tcir is further converted to pIWP in g/m^2 using a modeled pIWP-Tcir relation, as in the MLS cloud ice retrieval.

A key parameter that characterizes *pIWP* is the bottom height of the partial column, which can be roughly estimated from the modeled clear-sky radiances using atmospheric temperature lapse rate (7.5 km) [Table 1-3]. These clear-sky MW T_b represent, to the first order, the upper-tropospheric blackbody emission: the colder the MW T_b, the higher the emission height. For example, the MLS 640-

GHz clear-sky T_b is ~205K in the tropics, which corresponds to a blackbody temperature of T=220K. Assuming an atmosphere with the scale height of 7 K/km and a surface temperature T_s=300K, one would obtain a bottom height of ~11 km for the 640-GHz limb sounding channel. By the similar token, the bottom height for IceCube 883-GHz cloud ice is ~8 km, slightly lower than MLS 640 GHz but higher than MLS 240 GHz, which suggests that the 883-GHz cloud ice should fall between MLS 640 and 240 GHz *pIWP* in terms of column amount.

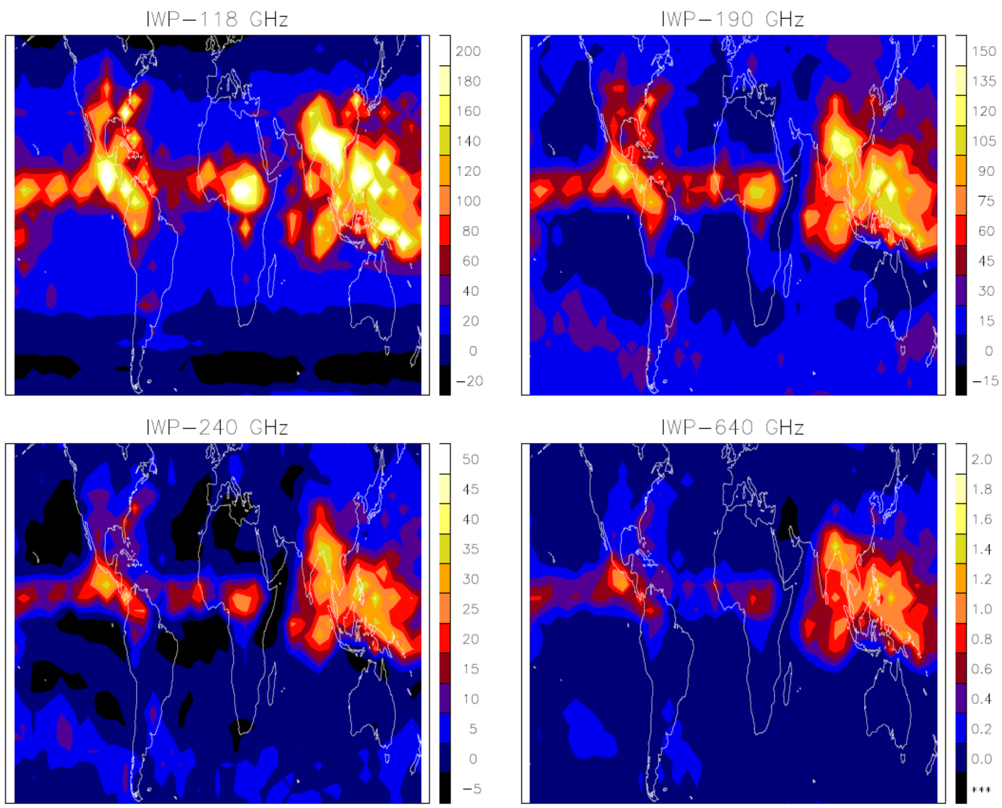

Fig. 1-20. Aura/MLS cloud pIWP maps for July-September 2017 in the same latitude range. Four MLS channels can observe cloud ice from limb sounding geometry, each of which corresponds to a different partial column height [Table 3]. In addition, the higher the frequency, the more sensitivity of MLS radiance to small cloud particle scattering. Combined effects from scattering sensitivity and penetration depth determine the observed pIWP [Wu et al., 2009].

The first global 883-GHz cloud ice map was obtained by IceCube during its operation in July-September 2017 [Fig. 1-19]. It represents the unique upper-tropospheric cloud ice amount detected by a sensor that has sensitivity between traditional MW and IR instruments from space. The IceCube-measured cloud ice is a column amount roughly from heights above 8 km. Despite much fewer samples taken during this observation period, IceCube produces a cloud ice morphology similar to MLS *pIWP* maps [Fig. 1-20], in particular, to the MLS 640

GHz, where both sensors have a similar frequency sensitivity to ice cloud scattering. There are three prominent peaks in the IceCube map that come from tropical deep convection in the intertropical conversion zone (ITCZ). The Pacific peak is strongest, followed by one over the central America and tropical Africa. The similar relative strengths are seen in the MLS 640 GHz cloud ice map.

Compared to the MLS *pIWP* in the extratropics [Fig. 1-20], IceCube's 883-GHz radiometer observes more cloud ice than that from MLS 640 GHz but less than MLS 190 and 240 GHz observations. IceCube's nadir/slant viewing geometry and higher frequency (better sensitivity to smaller particles) gives it deeper penetration into the upper tropopause than MLS 640-GHz limb sounding. Therefore, the additional cloud ice seen by IceCube is consistent with the slightly deeper penetration in the extratropics. However, MLS 190 and 240 GHz channels, which make even deeper penetration (~7km), have larger *pIWP* values than IceCube in the extratropics as expected.

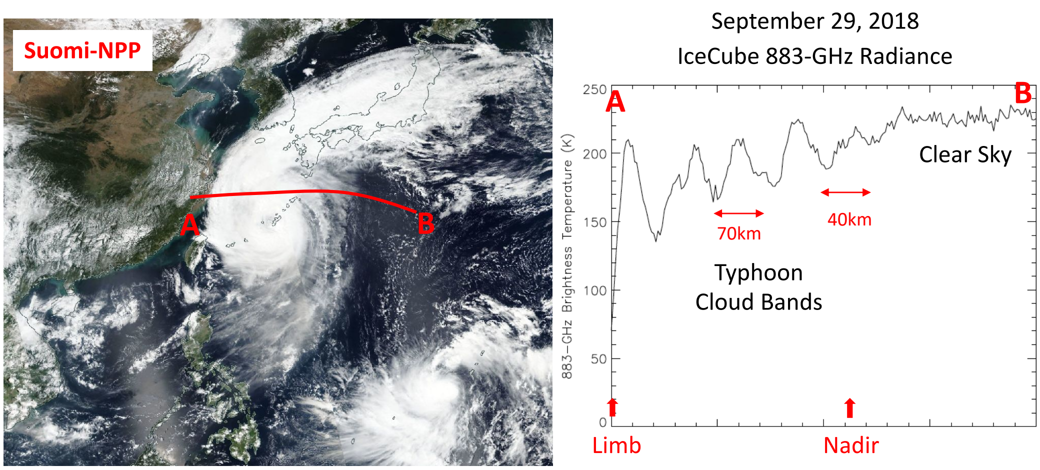

Fig. 1-21. IceCube flew over Typhoon Trami at 0320 UTC on September 29, 2018 during its reentry into the atmosphere. The 883-GHz cloud radiometer captured several cloud bands on the top of typhoon cloud deck before the scan reached Earth's limb at point A. The sharp drop in radiance to ~70 K at point A, indicating the field-of-view at limb viewing, is in fact the clear-sky portion of the system in China.

On September 29, 2018, four days before its reentry, IceCube was at an orbital altitude of ~200 km and made a scan across Typhoon Trami just south of Japan [Fig. 1-21]. IceCube's measurements are sensitive to most of upper-tropospheric cloud ice spun off from the typhoon eyewall. The oscillatory radiance features seen by IceCube are the manifestation of ice scattering from spiral cloud bands and Trami's cloud top deck. At the 200-km orbit, the IceCube's footprint is 5.9 km at nadir with 3-km measurement spacing. However, the footprint size doubles at the scan angle of 45 ° from nadir. Because of the variable sampling resolution, the oscillatory radiance features are associated with different horizontal scales of cloud bands in the typhoon. Typhoon Trami reached Category 5 intensity in the western Pacific Ocean on September 25, becoming the sixth

Category 5 tropical cyclone in 2018. According to the statistics from NOAA's National Hurricane Center and the U.S. Navy's Joint Typhoon Warning Center, Earth had an average of 5.1 Category 5 storms per year between 1990 and 2017.

1.6 Conclusion Remarks

IceCube is the first CubeSat built by GSFC at the time (i.e., 2014) when commercial CubeSat providers were immature and only spacecraft subsystems and components were available. It was a pathfinder at NASA to put a 3U flight system quickly so as to demonstrate the commercial low-cost 883-GHz cloud receiver technology. Thus, the IceCube instrument and spacecraft development was on an unusually fast schedule (2.5 years) and tight budget, compared to normal NASA flight projects. The IceCube spacecraft integration and test revealed numerous reliability issues with COTS parts and subsystems, for which some re-engineering and rework were needed. Relying on NASA's system engineering approach, the project was able to identify and mitigate the mission-critical risks through expert advice, vigorous testing in targeted subsystems/components, and small, swift working-group activities. In the instrument and CubeSat development, the "good enough" and "should-work" principles were adopted to balance mission risks in cost and schedule management. Prior to delivery, IceCube was tested thoroughly as a "Class D-minus" mission in a flight-like thermal vacuum environment to verify instrument and system functionality. The final delivered system was a product with some medium risks, with the top two risks associated with mechanisms in solar panel deployment and battery inhibit switches.

IceCube demonstrated the CubeSat spinning capability at altitudes > 200 km with a spin rate as high as 3.3 dps. To maximize the spacecraft's power input, IceCube operation was configured to keep the solar panels facing at the Sun all times during the day. The spacecraft spins around the Sun vector during daylight and around the local magnetic field vector at night. The spin produces periodic views of cold space for radiometric calibration of the 883-GHz cloud radiometer.

The spaceflight performance of the IceCube spacecraft and instrument exceeded their expectations. The project met all mission objectives for 883-GHz technology demonstration, and continued to accumulate knowledge about long-term stability and performance of the CubeSat and the cloud radiometer. The 15-month flight data show that the 883-GHz commercial radiometer can last for a long period of time and maintain a good sensitivity at its designed operational temperature. This instrument longevity has an important implication for both Earth and planetary science missions when long-period observations and long journeys are needed.

Inflight operation experiments also confirmed that the 18-W IceCube EPS was able to support 24/7 operation of the 5.6-W payload. The 883-GHz radiometer can be powered on continuously without over-discharging its battery during eclipse. The instrument would reach an equilibrium temperature of T_p

~38°C in the 24/7 mode. For good-quality cloud observations, IceCube operation employed a thermal-control mode since October 2017, in which T_p was capped at 30°C. Thanks to the low solar activity, IceCube's orbital lifetime was significantly longer than the MinXSS-1 3U CubeSat that was released from the ISS one year earlier [Mason et al., 2017]. IceCube reentered the atmosphere on Oct 3, 2018 [Fig. 1-22].

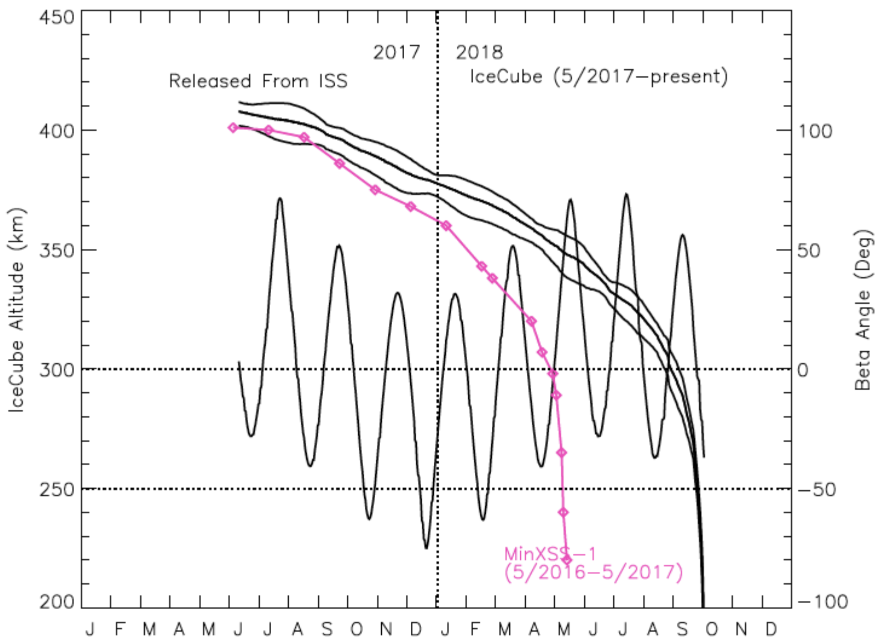

Fig. 1-22. IceCube reentered the atmosphere on Oct. 3, 2018 after ~16 months from the ISS release. The apogee, perigee, and average altitude of IceCube's elliptical orbit were derived from the TLE data and plotted separately. For comparison, the average altitude of the MinXSS-1 orbit (pink) is also shown. It had a lifetime of ~12 months after release from the ISS about one year earlier than IceCube when solar activity was slightly higher. The last science data from IceCube was acquired on September 29 when it was at ~200 km, showing that the spacecraft was spinning normally.

The IceCube 883-GHz cloud radiometer was essentially a free-running receiver without internal calibration targets. It relied on periodic views of cold space and the power-cycling MLA of the receiver for radiometric calibration. The spinning CubeSat provided frequent space views, which were sufficient to track and model the receiver's background count variations. The power-cycling MLA receiver operation allowed separation of the instrument frontend and backend noise contributions, and effective removal of complex backend noise variations in the *Ant-Ref* count differences. In the final product, the 883-GHz radiances have been calibrated to ~3K. These calibrated radiances produced the first 883-GHz cloud ice map validated by MLS observations during the same period.

In summary, the successful IceCube spaceflight and submm-wave technology demonstration have enabled a new remote sensing capability for future cost-constrained science missions with:

- Low-cost, space-qualified instruments at frequencies up to 883 GHz;
- Fast-track, risk-taking exploration with focused science objectives; and
- Cost-effective implementation of a SmallSat/CubeSat constellation where high spatiotemporal sampling is needed.

1.7 Acknowledgments

The IceCube project was supported by NASA's Science Mission Directorate (SMD) and Earth Science Technology Office (ESTO), Goddard Space Flight Center (GSFC), NASA's CubeSat Launch Initiative (CSLI), and the International Space Station (ISS). IceCube's success was attributed to the hard work, perseverance and dedication of many individuals throughout its development and operation. These team members include Mustafa Aksoy, Marion August, Behnam Azimi, Jonathan Bensman, Benjamin Cervantes, Michael Choi, Alexander Coleman, Caitlyn Cooke, Brian Corbin, Theodore Daisey, Cornelis Du Toit, Carlos Duran-Aviles, Lula Fetter, Brooks Flaherty, Jie Gong, Henry Hart, Scott Heatwole, Jeffrey Hesler, Kevin Horgan, John Hudeck, Derek Hudson, Brad Lafata, Christopher Lewis, Jason Li, Yuping Liu, Daniel Lu, Jared Lucey, Shawn Macmurphy, William Mast, Steven Retzloff, Juan Rodriguez-Ruiz, Joel Simpson, Michael Solly, Robert Stancil, Melyane Ortiz-Acosta, Armi Pellerano, Eric Pollack, Christopher Purdy, and Mark Wong.

1.8 References

Bosilovich, M. G., et al. (2015): MERRA-2: Initial evaluation of the climate. Technical Report Series on Global Modeling and Data Assimilation, Vol. 43, NASA Tech. Rep. NASA/TM–2015–104606, 139 pp. [Available online at https://gmao.gsfc. nasa.gov/pubs/docs/Bosilovich803.pdf.]

Buehler, et al, (2012), "Observing ice clouds in the submillimeter spectral range: the CloudIce mission proposal for ESA's Earth Explorer 8," Atmos. Meas. Tech., 5, 1529–1549.

Dowling, D. R. and L. F. Radke (1990), "A summary of the physical properties of cirrus clouds," Jour. Appl. Meteor., vol. 29, pp. 970-978.

Eliasson, S., et al. (2011), "Assessing observed and modelled spatial distributions of ice water path using satellite data," Atmos. Chem. Phys., 11, 375–391, doi:10.5194/acp-11-375-2011.

Eriksson, P., M. Ekstrom, B. Rydberg, D. L. Wu, R. T. Austin, and D. P. Murtagh, 2008: Comparison between early Odin-SMR, Aura MLS and CloudSat retrievals of cloud ice mass in the upper tropical troposphere. Atmos. Chem. Phys., 8, 1937–1948, doi: 10.5194/acp-8-1937-2008.

Evans, K. F., S. J. Walter, A. J. Heymsfield, G. M. McFarquhar (2002): Submillimeter-wave cloud ice radiometer: Simulations of retrieval algorithm performance. J. Geophys. Res. 107: 2.1–2.21.

Evans, K.F., et al. (2012), "Ice hydrometeor profile retrieval algorithm for high frequency micro-wave radiometers: application to the CoSSIR instrument during TC4," Atmos. Meas. Tech., 5, 2277-2306. doi:10.5194/amt-5-2277-2012.

Gong, J., and D. L. Wu (2014), CloudSat-constrained cloud ice water path and cloud top height retrievals from MHS 157 and 183.3 GHz radiances, Atmospheric Measurement Techniques, **7 (6):** 1873-1890

Hesler, J. (2004) "Compact Terahertz Heterodyne Receivers," NASA SBIR Phase II Final Report, Contract: NAS5-02107.

IPCC, (2013): Climate Change 2013: The Physical Science Basis. Contribution of Working Group I to the Fifth Assessment Report of the Intergovernmental Panel on Climate Change [Stocker, T.F., D. Qin, G.-K. Plattner, M. Tignor, S.K. Allen, J. Boschung, A. Nauels, Y. Xia, V. Bex and P.M. Midgley (eds.)]. Cambridge University Press, Cambridge, United Kingdom and New York, NY, USA, 1535 pp.

Jiang, J. H., et al. (2012), Evaluation of cloud and water vapor simulations in CMIP5 climate models using NASA "A-Train" satellite observations, J. Geophys. Res., 117, D14105, doi:10.1029/2011JD017237.

Li, J.-L. F., D. E. Waliser, G. Stephens, S. W. Lee (2016), Characterizing and understanding cloud ice and radiation budgets in global climate models and reanalysis, AMS monograph Attribute to Late Professor M. Yanai, Chap.13. http://dx.doi.org/10.1175/AMSMONOGRAPHS-D-15-0007.1

Mason, J.P., et al. (2017), MinXSS-1 CubeSat On-Orbit Pointing and Power Performance: The First Flight of the Blue Canyon Technologies XACT 3-axis Attitude Determination and Control System, Journal of Small Satellites, 6, 651

Randall, D. A., et al. (2007), "Climate models and their evaluations" in Climate Change 2007: The Physical Sciences Basis, Contribution of Working Group I to the Fourth Assessment Report of the Intergovernmental Panel on Climate Change, edited by S. Solomon et al., chap. 8, pp. 589–662, Cambridge Univ. Press, Cambridge, U. K.

Schlecht, E., et al. (2004), "Capability of THz sources based on Schottky diode frequency multiplier chains," Microwave Symposium Digest, IEEE MTT-S International, 6-11 June 2004, vol.3, pp 1587-1590.

Stephens, G. L., et al. (2008), CloudSat mission: Performance and early science after the first year of operation, J. Geophys. Res., 113, D00A18, doi:10.1029/2008JD009982.

Thébault, E., et al., et al. (2015): International Geomagnetic Reference Field: the 12th generation. Earth, Planets and Space 2015, 67:79.

Thomas, B., et al., (2008): "Design of an 874 GHz biasable sub-harmonic mixer based on MMIC membrane planar Schottky diodes," In proceeding of 33rd International Conference on Infrared, Millimeter and Terahertz Waves. doi:10.1109/ICIMW.2008.4665424.

Thomas, B., et al., (2010): "A Broadband 835–900-GHz Fundamental Balanced Mixer Based on Monolithic GaAs Membrane Schottky Diodes," IEEE

Trans. Microwave Theory and Techniques, doi:10.1109/TMTT.2010.2050181.

Waliser, D. E., et al. (2009), “Cloud ice: A climate model challenge with signs and expectations of progress,” J. Geophys. Res., 114, D00A21, doi:10.1029/2008JD010015.

Wu, D. L., W. G. Read, A. E. Dessler, S. C. Sherwood, and J. H. Jiang, UARS MLS Cloud Ice Measurements and Implications for H2O Transport near the Tropopause, *J. Atmos. Sci.*, 62 (2): 518-530 FEB 2005.

Wu, D. L., J. H. Jiang, and C. P. Davis (2006), EOS MLS cloud ice measurements and cloudy-sky radiative transfer model, IEEE Trans. Geosci. Remote Sens., 44(5), 1156– 1165.

Wu, D. L., and Coauthors, 2008: Validation of the Aura MLS cloud ice water content measurements. J. Geophys. Res., 113, D15S10, doi:10.1029/2007JD008931.

Wu, D. L., et al. (2009), Comparisons of global cloud ice from MLS, CloudSat, and other cor-relative data sets. J. Geophys. Res. (CloudSat special section), doi:10.1029/2008JD009946.

Zhang, Z. and B. Monosmith (2008), “Dual-643 GHz and 874 GHz Airborne Radiometers for Ice Cloud Measurements,” IEEE Int. Geoscience and Remote Sensing Symposium (IGARSS), Boston, 7-11 July 2008, vol.2, pp.1172-1175.

Zhao, L. and F. Weng (2002): Retrieval of ice cloud parameters using the Advanced Microwave Sounding Unit (AMSU). J. Appl. Meteor.,41, 384-395.